NUREG/CR-1405
BNL-NUREG-51180
AN, R-7

THE NACOM CODE FOR ANALYSIS OF POSTULATED SODIUM SPRAY FIRES IN LMFBRs

S.S. Tsai

Manuscript Completed - September 1979
Date Published - March 1980

ENGINEERING AND ADVANCED REACTOR SAFETY DIVISION
DEPARTMENT OF NUCLEAR ENERGY
BROOKHAVEN NATIONAL LABORATORY
UPTON, NEW YORK 11973

PREPARED FOR
U.S. NUCLEAR REGULATORY COMMISSION
WASHINGTON, D.C. 20555
UNDER INTERAGENCY AGREEMENT DE-AC02-76CH00016
NRC FIN NO. A-3000

Available from
GPO Sales Program
Division of Technical Information and Document Control
U.S. Nuclear Regulatory Commission
Washington, D.C. 20555
and
National Technical Information Service
Springfield, Virginia 22161

ABSTRACT

An analysis of potential sodium spills and fires in liquid metal fast breeder reactors has been made to assess the maximum equipment cell loading conditions. A computer code called NACOM (sodium combustion) has been developed at Brookhaven National Laboratory (BNL) to analyze sodium spray fires. This report contains a detailed description of physical models used in this code as well as programming aspects. The single droplet combustion model and the model describing the droplets' motion are verified. Comparisons between NACOM predictions and SPRAY-3A predictions of the Atomics International (AI) LTV Jet Tests are made. Good agreement is found between the NACOM predictions and the experimental data. NACOM predictions of the pressure rise are more accurate than SPRAY-3A predictions for most of the cases studied. The code has been verified for oxygen concentrations ranging from 0 to 21%. NACOM utilizes more realistic single droplet and spray combustion models than SPRAY-3A. Moreover, NACOM does not utilize adjustable parameters for the burning rate equations, contrary to the approach taken with SPRAY-3A. Thus, the NACOM code is a more reliable code for use in the analysis of large-scale sodium spray fires in LMFBR containment cells.

TABLE OF CONTENTS

LIST OF FIGURES

LIST OF FIGURES (Cont'd)

LIST OF TABLES

NOMENCLATURE

Symbol	Definition
A	Total cell surface area
B	Transfer number defined in Equation (4.6)
C	Molar Density
C_d	Drag coefficient
C_f	Empirical constant defined in Equation (4.8)
C_p	Gas mixture heat capacity
$C_{v,g}$	Specific heat of the gas at constant volume
$C_{v,w}$	Specific heat of the walls
D	Droplet diameter
$\bar{D}$	Volume mean diameter
D_d	Diffusion coefficient
D_i	Initial droplet diameter
D_{max}	The largest group size
D_{min}	The smallest group size
g	Gravitational acceleration
h_{fg}	Heat of evaporation
h	Heat transfer coefficient at the walls
H_c	Heat of combustion
i	Stoichiometric ratio
k	Gas mixture thermal conductivity
K	Burning rate coefficient or evaporation constant
$\dot{m}$	Droplet mass burning rate
$\dot{m}_f$	Falling droplet mass burning rate
m_g	Total mass of gas inside a containment cell
$\dot{m}_\ell$	Sodium leak rate
$\dot{m}_s$	Spray mass burning rate
m_w	Total mass of the walls

NOMENCLATURE (Cont'd)

Symbol	Definition
$\dot{m}_z$	Rate of sodium mass crossing the z plane
N	Total number of droplets
Nu	Nusselt number
P	Cell pressure
Pr	Prandtl number
q_g	Rate of heat transfer from a single droplet to the gas
Q_g	Rate of heat transfer from the sodium spray to the gas
Q_w	Rate of heat transfer from the gas to the walls
R	Universal gas constant
R_v	Volume fraction of spray which contains droplets of diameters smaller than D
Re	Reynolds number
Sc	Schmidt number
t,t'	Time
T_f	Flame temperature
T_g	Average gas temperature
T_s	Droplet temperature
T_w	Wall temperature
V	Volume of the cell
V_f	Droplet falling velocity
V_H	Reaction rate constant for water vapor reaction
V_o	Reaction rate constant for oxygen reaction
Y	Ambient oxygen mole fraction
z	Coordinate measured vertically downward from the ceiling

NOMENCLATURE (cont'd)

Greek Symbol	Definition
ρ	Density
ρ_g	Density of the gas
ρ_{Na}	Density of sodium

1. INTRODUCTION

Sodium spills and fires in the primary and secondary systems of a liquid metal fast breeder reactor (LMFBR) pose a potential threat to the safe operation of the plant. In current LMFBR designs, engineered safety features, such as inerted primary system cells, nitrogen flooding system, are provided to prevent leaking sodium from reaching flammable combustion. However, in the event of large-scale sodium spills, pressure and temperatures in an inerted cell may increase substantially because of a large amount of sensible heat contained in the leaking sodium, even though there is no flammable combustion. In oxygen-enriched atmospheres, the leaking sodium will chemically react with oxygen and release heat of combustion, resulting in pressure-temperature transients in containment cells.

Of the two basic types of sodium fires, i.e., spray and pool fires, spray fires are generally considered to be more severe than pool fires in terms of equipment cell thermal transients. This is due to the fact that a sodium spray always burns at a higher rate than a sodium pool containing the same amount of sodium because the spray burns in a highly divided state, namely, droplet form.

Sodium spray fires are often postulated to result from pipe breaks. The sodium coming out of the break is usually assumed to eject upward, impinging on the ceiling of a containment cell. A liquid film will form on the ceiling and then break up to form droplets. The falling droplets form a sodium spray. The spray will chemically react with oxygen in the cell atmosphere, transferring the heat of combustion to the cell gas. This leads to pressure-temperature transients in the cell. It is necessary to assess the severity of the equipment cell thermal transients in order to determine whether adequate structural margins are provided for the cell. To assess the transients, a reliable analytical tool is required.

Sodium spray fires involve complicated combustion and transport processes which are not yet fully understood. For example, the effects of droplet interaction, oxygen depletion in the spray zone, and water vapor on spray burning remain largely unknown. The conventional approach to modeling sodium spray fires starts with the modeling of single droplet heat transfer and combustion. The burning rate of a single droplet is predicted by using a vapor-phase combustion theory. The spray is usually visualized as a cluster of droplets and hence the spray burning rate is the sum of the individual droplet burning rates. In determining the spray burning rate, the effects of droplet interaction, nonuniformity of gas temperature across the spray zone, and depletion of oxygen inside the spray zone are usually neglected.

To date a number of computer codes have been developed to analyze sodium spray fires. Of all these codes SPRAY[1] has been widely used in the United States. The early version of SPRAY was designed to deal with spray fires in low oxygen concentrations (less than two volume percent*). The latest version of the code, SPRAY-3A[2], introduced adjustable parameters in the burning rate equations. The reaction rate constant V_O was used for oxygen reactions and the reaction rate constant V_H for water vapor reactions. The values of V_O and V_H were selected by fitting the code's calculational results with experimental data obtained from 16 Atomics International (AI) sodium spray tests. As a result of this best fit, the values of V_O and V_H were chosen as 85 and 1500, respectively. Even with the introduction of these two parameters, SPRAY-3A predictions of the AI experiments in the intermediate oxygen concentrations between 2 to 5% are poor.

*Throughout the text the indicated percentage of oxygen designates volume percent.

Another frequently used sodium spray fire code is SOMIX.[3] SOMIX-1 basically retains the SPRAY vapor-phase combustion model, with a major improvement in the cell gas circulation model. It seems that SOMIX-1 has experienced difficulties in predicting spray fires in high oxygen concentrations similar to the difficulties experienced in the early development of SPRAY. Instead of using the vapor-phase combustion model, SOMIX-2 adopted Krolikowski's diffusion model[4] for calculating the sodium burning rate in an air atmosphere. In SOMIX-2, sodium burning was based on the rate at which oxygen diffuses to the burning zone. Krolikowski's model does not consider sodium vapor diffusion to the burning zone, and therefore underestimates the sodium burning rate.

Both SPRAY and SOMIX seems to have difficulty in predicting spray fires in high oxygen environments, where the accuracy of the combustion model is important. SPRAY attempted to overcome this difficulty by means of adjustable parameters, while SOMIX reverted to the early developed Krolikowski's model in order to obtain better agreement with experimental data. It is, therefore, imperative to develop a sodium spray fire code with a reliable combustion model.

A sodium spray fire analytical model, NACOM, was recently developed at BNL. NACOM uses an established single droplet vapor-phase combustion theory, which is different from those used in SPRAY and SOMIX. The theory is well established for combustion of hydrocarbon fuel droplets. It is expected to be equally applicable to combustion of sodium droplets because the combustion of both hydrocarbon fuel and sodium droplets follows the "D^2" law.[5]

The SPRAY code uses the surface mean drop size, which is derived from the volume mean drop size and a log-normal drop size distribution, to compute the droplet burning rate and heat transfer from the droplets to the cell gas. Analysis with SOMIX has shown that the use of only one drop size could lead to

considerable error in the prediction of the pressure rise. In contras., NACOM employs a drop size distribution to calculate the spray burning rate and is therefore expected to yield better results.

Both SPRAY and SOMIX assume that sodium droplets burn in the vapor phase immediately after they appear at the ceiling. The preignition phase of the droplets has been ignored. The neglect of preignition combustion will overestimate the droplet burning rate and pressure. In contrast, NACOM includes a preignition model developed earlier at BNL.[6] These improvements and other features of the NACOM code will be discussed in the following sections.

2. CHARACTERISTICS OF SODIUM COMBUSTION

Sodium is a soft silvery metal, which melts at 98°C. Sodium burns readily in an air atmosphere, especially in the presence of water vapor, forming various oxides. Only two oxides, namely, sodium monoxide and peroxide, are found to be abundant in the reaction products. Sodium monoxide, Na_2O, melts at 1,132°C and decomposes at 1,950°C and may be formed in the following chemical reaction

$$2Na + \tfrac{1}{2}O_2 \rightarrow Na_2O. \qquad (2.1)$$

During this exothermic reaction 2,195 cal/g of combustion heat is released. With excess oxygen at 238 to 400°C, the monoxide is oxidized to sodium peroxide, Na_2O_2. Sodium peroxide melts at 674°C and decomposes at about 1,627°C. The peroxide formation may be represented by

$$2Na + O_2 \rightarrow Na_2O_2. \qquad (2.2)$$

During this reaction, 2,500 cal/g of combustion heat is released.

In the presence of water vapor in air, sodium hydroxide may be formed by the following reaction

$$2Na + 2H_2O \rightarrow 2NaOH + H_2. \qquad (2.3)$$

Sodium does not react with nitrogen at all known temperatures. However, in the presence of electric discharge, sodium may react with nitrogen to form the nitride or the azide.

Sodium fires are characterized by flames and dense clouds of white smoke. The sodium in a fire is not entirely consumed to form smoke; most of the sodium remains as residue in the form of sodium oxide and unreacted sodium. Reaction

products in the residue and smoke contain both sodium peroxide and monoxide. In excess oxygen, the sodium peroxide is the principal reaction product; in excess sodium, the sodium monoxide predominates; between these two extremes, substantial quantities of both oxides could be formed.

At oxygen concentrations higher than 5%, sodium spray fires are characterized by incandescence, dense smoke, and rapid pressure increase. At or below 5% oxygen, there is insufficient oxygen to sustain a flammable combustion or incandescence. However, the smoke occurs at oxygen concentrations down to 0.1%.

3. PREVIOUS WORK ON SODIUM SPRAY FIRES

3.1 Sodium Spray Fire Experiments

In 1952 Mangold and Tidball[7] reported sodium spray fire tests conducted in a semi-cylindrical chamber. In the tests, 14.5 to 88.9 kg of sodium at 454°C were forced through a nozzle and driven into the chamber. The tests were performed in various oxygen concentrations ranging from 2.75 to 21%. A maximum chamber pressure rise of 0.48 atm was measured in 21% oxygen.

Hines and Kelley[8] have reported tests in which 454°C sodium was sprayed into a 532 ℓ container. They found that the maximum pressure decreased with decreasing initial oxygen concentrations. In these tests, a maximum pressure rise of 2.59 atm was obtained in an air atmosphere.

In 1958 Humphreys[9] performed a small-scale experiment in which 399°C sodium was driven into a sealed vessel filled with air. A peak pressure rise of 5.78 atm was recorded.

Subsequently, Gracie and Droher[10] performed sodium spray experiments in a rectangular chamber at low oxygen concentrations. A maximum pressure rise of 0.12 atm in 2% oxygen was measured.

Charak and Smith[11] have reported a series of sodium spray tests in which 1-2 grams of sodium at 649°C were injected into an air-filled chamber. The maximum pressure rise found in the tests was ~5.44 atm.

Krolikowski[4] injected 10 g of sodium at 413°C into a chamber filled with N_2-O_2 mixtures. A maximum pressure of 3.06 atm was recorded.

More recently, Atomics International conducted a series of sodium spray tests.[12] Commercial spray nozzles were mounted on top of a spray test vessel. Pressure rises in the test vessel were recorded for sodium spray in various oxygen concentrations. Subsequently, a series of sodium spray dispersal tests

were conducted in the Large Test Vessel[13] (LTV). In the tests, sodium sprays were formed by directing sodium jets upward against an impact plate. Large sodium drops were produced in the tests. A maximum pressure of ~0.27 atm in 5% oxygen was recorded in the tests.

3.2 Single Sodium Drop Tests

Richard et al.[5] performed stationary sodium drop burning experiments in various oxygen concentrations, with initial droplet diameters of 1, 2, and 3 mm. He found that the burning of the sodium drops follows essentially the "D^2" law that has been established for the combustion of hydrocarbon fuel droplets, i.e., the square of the droplet diameter decreases linearly with time during combustion.

Subsequently, Atomics International conducted both stationary and falling drop tests in the Laboratory Drop Modeling (LDM) test apparatus.[14] In the stationary drop tests, the droplet burning rates for 6-7 mm droplets were measured. In the falling drop tests, the distance at which the droplet reaches full burning and the fraction of droplet mass burned in a 14.73 meter fall distance were recorded.

4. MODELING OF SODIUM SPRAY FIRES

In this section, the physical models that are used in the NACOM code to simulate combustion of a sodium spray in a vessel will be discussed. The sodium spray is formed by directing a sodium jet upward against an impact plate situated at the top of the vessel. The spray contains numerous sodium drops. Therefore, the formulation of this sodium spray combustion problem must start with formulation of the combustion of single sodium droplets. It is a conventional practice to derive the spray combustion rate by summing up all the burning rates of the individual droplets. The Spalding single droplet vapor-phase combustion theory will be discussed first. Then the modification factor for the burning rate equation in forced convection experienced by a falling droplet will be introduced. Subsequently, Section 4.3 will be devoted to the discussion of the drag coefficient and solution to the equation of droplets' motion. With the introduction of a drop size distribution the spray combustion will be formulated in Section 4.5. Finally, the energy conservation equations for the walls and the gas inside the vessel will be discussed in Section 4.6.

4.1 Combustion Model for a Spherical, Stationary Droplet

Figure 1 shows the combustion of a stationary droplet in its final stage, i.e., steady state. The droplet is surrounded by a burning zone or flame zone. The sodium vaporizing from the droplet surface diffuses toward the burning zone from the surroundings. Both sodium vapor and oxygen burn instantaneously and stoichiometrically in the burning zone. The heat released by the combustion is fed back to the droplet surface and contributes to the vaporization of the sodium, thus sustaining the vapor-phase combustion.

In the conventional vapor-phase droplet combustion theory, it is often assumed that a single stationary, spherical, burning droplet is surrounded by a spherical, symmetrical burning zone. It is further assumed that all the fuel reaching the burning zone is burned instantaneously under steady state conditions. It follows that the burning rate of the fuel is controlled by the rate of evaporation of the liquid droplet, which, in turn, is determined by the rate of heat transfer to the droplet.

The mass burning rate, $\dot{m}$, of a droplet may be related to the rate of decrease in droplet size by

$$\dot{m} = -\frac{d}{dt}\left(\frac{\pi}{6} D^3 \rho\right) \tag{4.1}$$

where ρ is the density of the droplet, and D is the droplet diameter. Equation (4.1) may be rewritten as

$$\frac{d(D^2)}{dt} = -\frac{4\dot{m}}{\pi\rho D} . \tag{4.2}$$

It has been shown in numerous hydrocarbon fuel drop combustion experiments that the square of droplet diameter decreases linearly with time. The proportionality constant, K, which is defined as $K \equiv -\frac{d(D^2)}{dt}$, is termed the burning rate coefficient or evaporation constant. Recently, Richard et al.[5] has experimentally verified that the combustion of sodium droplets also follows the "D^2" law. The evaporation constant obtained by Richard et al. for three furnace temperatures is shown in Fig. 2. It is seen from Fig. 2 that the evaporation constant is a linear function of the oxygen mole fraction. The mass burning rate may therefore be expressed in terms of K as

$$\dot{m} = \frac{\pi\rho K}{4} D \tag{4.3}$$

and the linear relationship between D^2 and t, namely,

$$D^2 = D_i^2 - Kt \tag{4.4}$$

is called the "D^2" law.

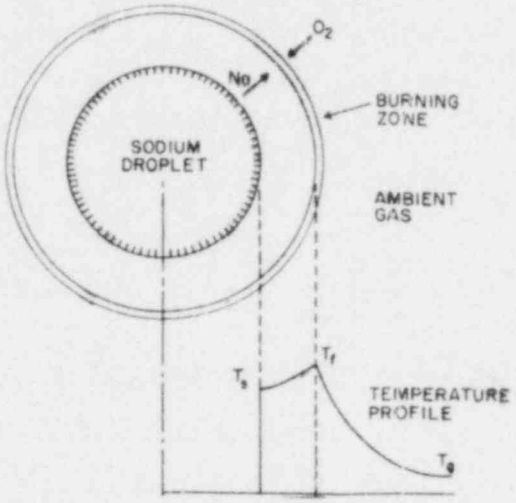

Figure 1. Schematic of a Burning Sodium Droplet

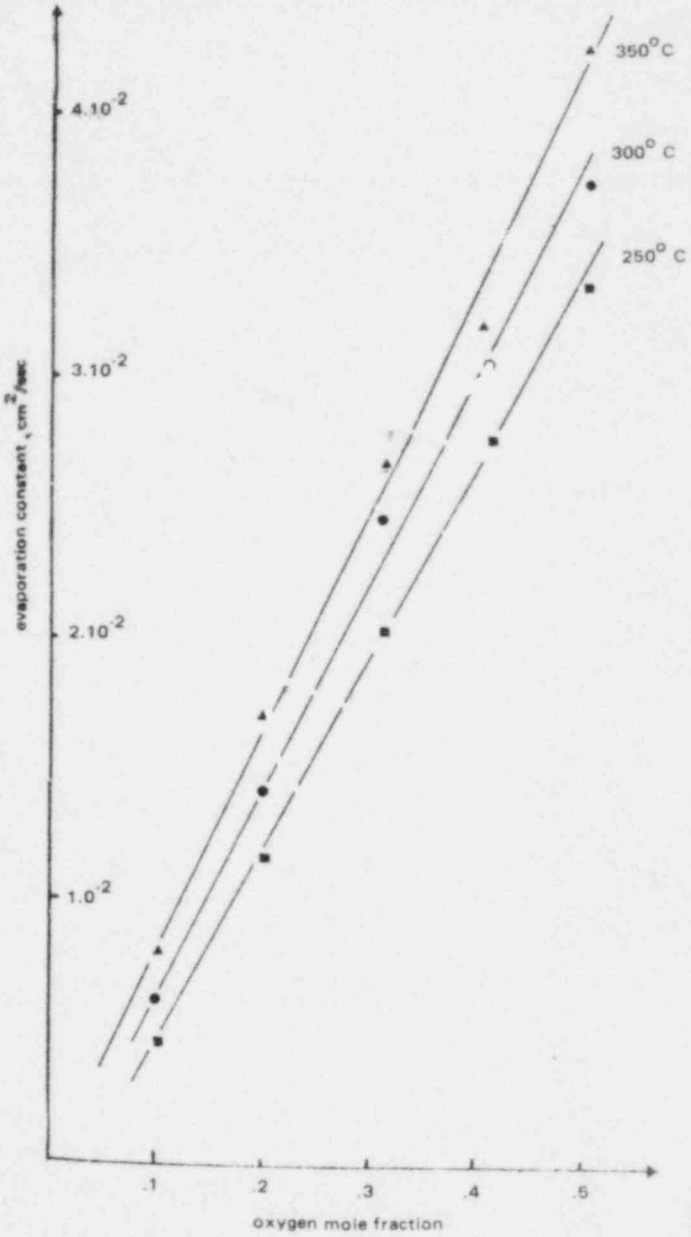

Figure 2. Dependence of Evaporation Constant K (at Different Temperatures) upon Mole Fraction of Oxygen Y

At present there are a number of quasi-steady-state vapor-phase droplet combustion theories. In general, these theories follow the "D^2" law. One of the established theories proposed by Spalding[15] gives

$$K = \frac{8k}{C_{p^o}} \ln (1+B) \tag{4.5}$$

where k is the gas mixture thermal conductivity, C_p is the gas mixture heat capacity, and the transfer number, B, is defined as

$$B \equiv \frac{1}{h_{fg}} \left\{ C_p (T_g - T_s) + \frac{H_c Y}{i} \right\} \tag{4.6}$$

Equation (4.5) has also been proposed at Atomics International during its early stage of model development effort.

4.2 Combustion Model for a Free-Falling Droplet

To apply the preceding theory to a free-falling droplet, the effect of forced convection on the droplet burning rate must be taken into account. The forced convection will cause the flame to deviate from spherical symmetry and increase the burning rate. It is very difficult to analytically obtain the droplet burning rate in forced convection. Therefore, most of the burning rate expressions for falling droplets are either empirical or semi-empirical correlations.

Both SPRAY and SOMIX assume that sodium droplets burn in the vapor phase immediately after they appear at the ceiling. The preignition phase of the droplets has been ignored. In the preignition period, a coarse film (or scale) of oxides is formed on the droplet surface by the surface oxidation process. Heat generated by the oxidation process is fed back to the droplet surface more easily than it is transferred to the gaseous atmosphere. This results in a rapid increase of the droplet temperature. Ignition of the droplet occurs

when the droplet ignition temperature is reached. A preignition oxidation model has been developed by Tsai.[6] In the model, the Ranz-Marshall correlation was used to predict oxygen diffusion to the droplet surface. The oxidation of sodium at the droplet surface will generate heat which is partly absorbed by the droplet and partly transferred to the cell gas. A governing equation was obtained by making an energy balance on the droplet, which was then solved for time and distance at which the droplet is ignited to reach full burning. The calculated droplet fall distance to reach full burning as a function of droplet diameter was found to be in good agreement with the LDM falling sodium drop test data.[6] The sodium droplet burning rate during preignition may be obtained from the oxygen flux and the stoichiometric ratio as

$$\dot{m}_f = \frac{\pi C D_d Y D}{i} \left(2 + 0.6\, Re^{1/2}\, Sc^{1/3}\right). \qquad (4.7)$$

After the droplet is ignited, the droplet is burned in the vapor phase. The burning rate for a stationary droplet burning in the vapor phase may be obtained from Equations (4.3) and (4.5). For a free-falling droplet, this burning rate should be modified by a multiplication factor that accounts for the forced convection effect. It has been found by various investigators that, on the basis of their experimental data, the droplet burning rate in forced convection may be related to the stationary droplet burning rate by

$$\dot{m}_f = \dot{m} \left(1 + C_f R_e^{1/2}\, Pr^{1/3}\right). \qquad (4.8)$$

The empirical constant C_f has been given values ranging from 0.24 to 0.31 by different investigators experimenting with different fuels. In the present analysis a value of 0.3 selected by Ranz and Marshall[17] is used.

The reason for choosing this value is that it correlates very well the data on the distance for a falling sodium drop to reach full burning during its preignition phase.[6] Substituting Equations (4.3) and (4.5) into Equation (4.8), we have

$$\dot{m}_f = \frac{2\pi k}{C_p} D \ (1+C_f Re^{\frac{1}{2}} \ Pr^{1/3}) \ \ell n \ (1+B). \qquad (4.9)$$

Agoston[18] used 0.31 and 0.22 as the values of the constant C_f for ethyl alcohol and n-butyl alcohol droplets, respectively. The agreement between Equation (4.9) with the chosen C_f values and experimental data is shown in Figs. 3 through 6.

An evaluation of physical properties that appear in Equations (4.7) and (4.9) is given in Appendix A.

4.3 Droplets' Motion

The equation of motion of an evaporating droplet differs from that of a rigid sphere by a term which accounts for the inertial force contributed by the mass flux effusing from the surface of the droplet. This affects the drag force on the droplet. When vapor effuses from the droplet surface, the skin drag decreases due to the thickening of the momentum boundary layer. In addition, combustion gases swept into the low pressure region within the wake of a burning droplet also reduce the form drag.

Considerable data on the steady-state drag coefficient for a rigid sphere are available, but very little data on the drag coefficient for an accelerating sphere exist. At high Reynolds numbers, it has been observed that flattening of the droplets causes an increase of the drag coefficient.

Due to the lack of reliable data and correlations, the mechanisms discussed above that affect the motion of a free-falling droplet will not be considered. Instead, the drag coefficient for a rigid sphere[1] is used in the present model of droplet motion, and may be written as

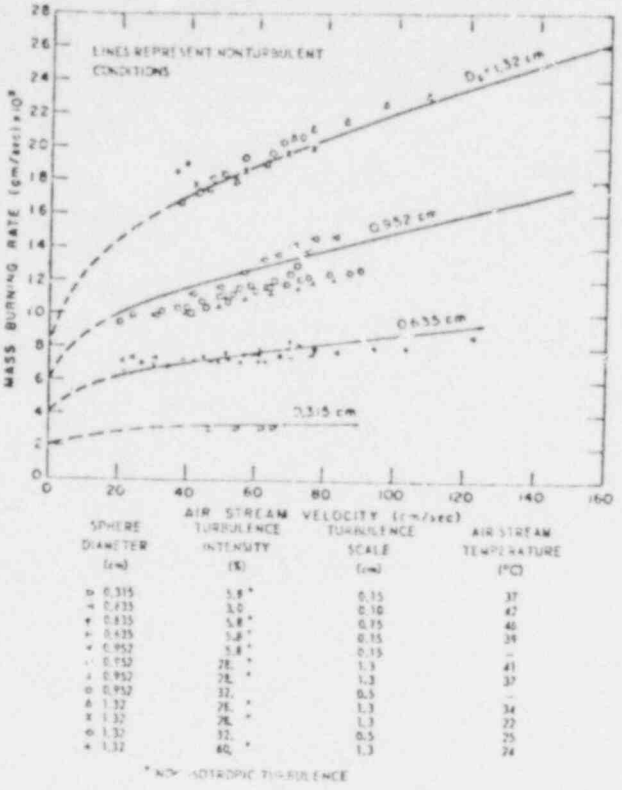

SPHERE DIAMETER (cm)	TURBULENCE INTENSITY (%)	TURBULENCE SCALE (cm)	AIR STREAM TEMPERATURE (°C)
0.315	5.8 *	0.15	37
0.635	3.0	0.10	42
0.635	5.8 *	0.15	46
0.635	5.8 *	0.15	39
0.952	5.8 *	0.15	–
0.952	28. *	1.3	41
0.952	28. *	1.3	37
0.952	32.	0.5	–
1.32	28. *	1.3	34
1.32	28. *	1.3	22
1.32	32.	0.5	25
1.32	60. *	1.3	24

* NON-ISOTROPIC TURBULENCE

Figure 3. Mass Burning Rates with and without Air Stream Turbulence. Fuel: n Butyl Alcohol

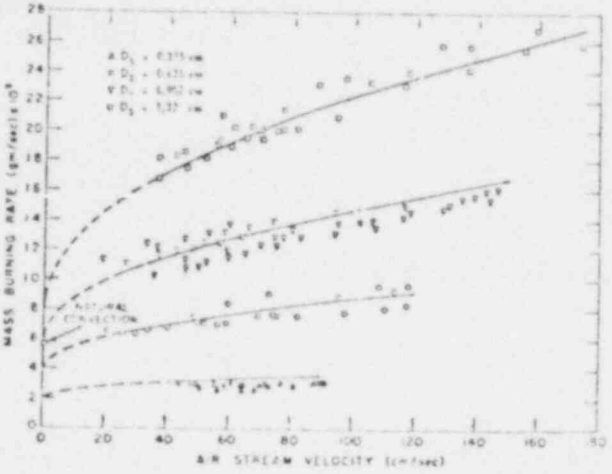

Figure 4. Mass Burning Rate as a Function of Sphere Diameter and Air Stream Velocity. Fuel: n-Butyl Alcohol; Air Stream Temperature: 26-40°C

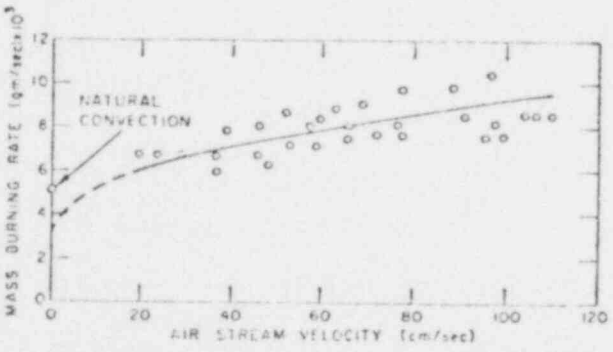

Figure 5. Mass Burning Rate as a Function of Air Stream Velocity. Fuel: Ethyl Alcohol (95.5 Per Cent by Weight); Sphere Diameter: 0.635 cm; Air Stream Temperature: 18-31°C

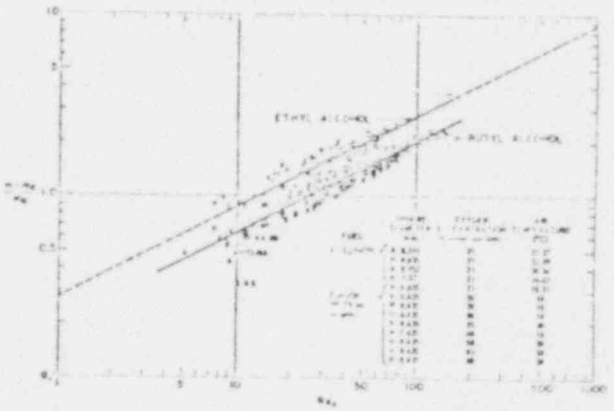

Figure 6. Correlations of Burning Rate Data

$$C_d = \begin{cases} 24/Re & Re < 0.1 \\ 2.6 + 23.71/Re & 0.1 \leq Re < 6 \\ 18.5/Re^{0.6} & 6 \leq Re < 500 \\ 4/9 & Re \geq 500. \end{cases} \quad (4.10)$$

The equation of motion of a burning droplet may be written as

$$\frac{dV_f}{dt} = g - \frac{3\rho_g V_f^2 C_d}{4\rho D} . \quad (4.11)$$

Upon substitution of Equation (4.10) into Equation (4.11), the latter can be integrated to yield V_f, which can then be used in Equations (4.7) and (4.9) to evaluate the falling droplet burning rates.

The Runge-Kutta method is used to solve Equation (4.11). The motion of the droplets is divided into equal time intervals. To avoid numerical instability at the beginning of droplets' motion, an asymptotic solution of Equation (4.11) at time zero is used in the initial phase of the motion, when the drag force is less than one hundredth of the gravitational force. The asymptotic solution is obtained from Equation (4.11) by letting V_f approach zero.

4.4 Drop Size Distribution

SPRAY uses a log-normal drop size distribution[1] to compute the surface mean drop diameter from the volume mean drop diameter. The surface mean drop diameter is then used to compute the droplet burning rate. The use of only one drop size could lead to substantial error in computing the spray burning rate.[19]

The log-normal drop size distribution used in SPRAY was first considered in the present analysis. However, it was found that it did not correlate with the drop

size distribution data obtained from Atomics International Jet Test No. 4 very well. Later, the Nukiyama-Tanasama correlation[19] was used, which seems to better correlate with the AI experimental data. The Nukiyama-Tanasama correlation may be written as

$$\frac{dR_v}{dD} = \left(\frac{3.915}{\bar{D}}\right)^6 \frac{D^5}{120} \exp\left(-\frac{3.915D}{\bar{D}}\right). \qquad (4.12)$$

Equation (4.12) is now used in the present version of NACOM. We note however that the NACOM code is not restricted to the use of the Nukiyama-Tanasama distribution. Other distributions can be accommodated.

4.5 Spray Combustion

The formulation of single droplet combustion is very straightforward. However, for a spray of liquid droplets, the parameters that affect spray combustion, such as the actual distribution of drop size, local number density of droplets, local oxygen concentration, and interaction between droplets are generally unknown. Due to depletion of oxygen in the spray zone, the oxygen concentration within the spray zone is lower than that outside the spray zone. However, the gas temperature is higher inside the spray zone than outside the spray zone because of heat released by combustion inside the spray zone. At present, the combustion model adopted in the NACOM code does not consider the variation of oxygen concentration over the spray zone. An average gas temperature is used in the code instead of assuming a temperature distribution over the spray zone. It is further assumed that there are no interactions among burning droplets, i.e., the combustion of each individual droplet in the spray is not affected by its neighboring droplets. Under this assumption, the single droplet combustion theory introduced in Sections 4.1 and 4.2 can be used to form the basis of the present spray combustion theory.

Consider sodium leaking with a mass flow rate $\dot{m}_\ell$ (t) into a cell of height H as shown in Fig. 7. It is assumed that the leaking sodium first impinges on the ceiling and then rains down to form a spray. The spray is assumed to consist of droplets obeying the Nukiyama-Tanasama drop size distribution. The droplets will burn away their mass during descent with the burning rate of the spray being the sum of the burning rates of all the droplets. There are two methods to formulate the spray burning rate. One is the Eulerian method and the other is the Lagrangian method. In the Eulerian method, a determination is made of the total burning rate of all the droplets which occupy an elemental volume in the spray zone at time t. A summation of all the contributions from all the elemental volumes is made to obtain the spray burning rate. It is difficult to implement this method to the present problem because the population of a group of droplets having a specific size changes from one elemental volume to another as a result of droplets' combustion. To circumvent this difficulty, the Lagrangian method keeps track of each group of droplets from the ceiling to the floor. The population of each size group is computed from the sodium leak rate and the Nukiyama-Tanasama size distribution. Since the method keeps track of every size group from its first appearance at the ceiling, the population of each group will not change during its descent although its average size will change because of combustion. The average size of each group at the time of interest is computed from the burning rate and its size at the last time step.

The spray burning rate is the sum of the burning rates of all the droplets, namely,

$$\dot{m}_s(t) = \int_{D_i} \int_{t'} \dot{m}_f \left(D\left(D_i, t', t\right), V_f\left(D_i, t', t\right)\right) d^2N \qquad (4.13)$$

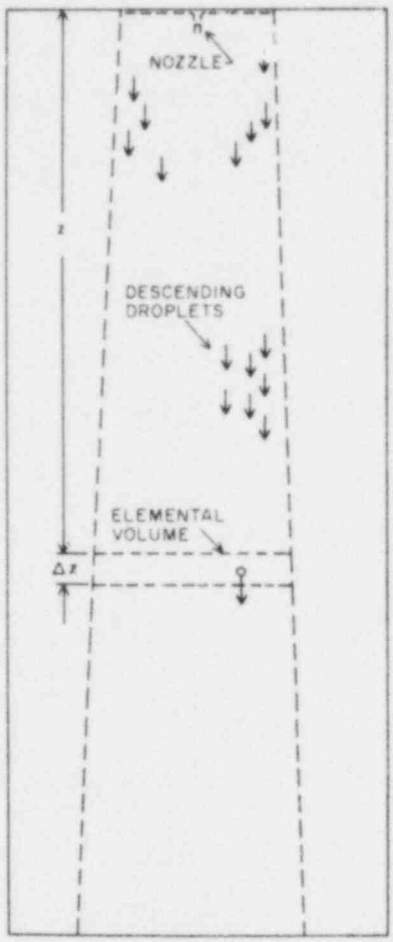

Figure 7. Schematic of Sodium Spray Combustion in a Vessel

d^2N is the number of droplets having diameters between D and D + dD, and having elevations between z and z + dz at time t. These d^2N droplets are originated from the ceiling at time t′, having initial diameters between D_i and $D_i + dD_i$. Since the Lagrangian method is used to follow a specific size group all the way from its appearance at the ceiling to the elevation z, the population of the group d^2N does not change with time until the whole group is completely burned up. Therefore, d^2N can be derived from the sodium leak rate and the drop size distribution as

$$d^2N = \frac{\dot{m}_\ell(t')}{\frac{1}{6}\pi D_i^3 \rho_{Na}} \frac{dR_v}{dD_i} dt' dD_i . \qquad (4.14)$$

Equation (4.14) can take any form of drop size distribution. When the Nukiyama-Tanasama correlation, Equation (4.12), is substituted into Equation (4.14), we have

$$d^2N = \frac{\dot{m}_\ell(t')}{\pi D_i^3 \rho_{Na}} \left(\frac{3.915}{\bar{D}}\right)^6 \frac{D_i^5}{20} \exp\left(-\frac{3.915 D_i}{\bar{D}}\right) dt' dD_i . \qquad (4.15)$$

The drop size D at time t can be computed from Equation (4.1) and the burning rate at the last time step. The velocity of a droplet at time t, which is needed to compute the burning rate $\dot{m}_f$, is obtained from the solutions of Equation (4.11).

During the preignition period, the preignition oxidation model, namely, Equation (4.7), is used to compute the burning rate $\dot{m}_f$. After the droplets reach full burning, the vapor-phase burning rate expression, namely, Equation (4.9) is used. At any instant the distances to reach full burning are computed for different drop sizes using the method described in Reference 6 with the additional consideration of heat transfer from the droplet to the gas.

To evaluate Equations (4.13) and (4.15) numerically, a constant time step, $\Delta t'$, and a constant range of drop size, ΔD_i, are selected. The range of integration with respect to drop size is chosen by determining the largest and smallest drop sizes. The largest and smallest group sizes, D_{max} and D_{min}, are determined by equating the total volumes of droplets in the two groups to 1% of the volume of the mean size group, i.e., $\left.\frac{dR}{dD}\right|_{D=D_{max}} = \left.\frac{dR}{dD}\right|_{D=D_{min}} = 0.01 \left.\frac{dR}{dD}\right|_{\bar{D}=D}$. The droplets between the groups which have the largest and smallest average drop sizes are divided into eleven groups. The integration is then approximated by the sum of the burning rates of all groups locating at different elevations, i.e.,

$$\dot{m}_s \tilde{=} \sum_i \sum_j \dot{m}_f \Delta N_{ij} \qquad (4.16)$$

where the i summation sums over all the size groups and the j summation over all the elemental volumes inside the spray zone.

4.6 Heat Transfer

4.6.1 Heat Transfer to the Gas

The combustion of the sodium spray will release heat of combustion to the surrounding gas. In the case of low oxygen concentrations in which combustion is insignificant, the sodium spray will transfer its sensible heat to the gas. When the spray is in vapor-phase combustion, it transfers part of the heat of combustion to the droplet surface to vaporize sodium and the remaining part of the heat to the surrounding gas. When sensible heat transfer is the dominant mode of heat transfer in low oxygen environments, the spray transfers heat to the gas simply by decreasing its temperature.

During the preignition period, the rate of heat transfer from a sodium droplet to the gas may be evaluated from the Ranz-Marshall correlation[17] as

$$q_g = \frac{k}{D} (2 + 0.6\ Re^{\frac{1}{2}}\ Pr^{\frac{1}{3}})\ (T_s - T_g). \tag{4.17}$$

After the droplets are ignited, the droplets are burning in the vapor-phase. The heat of combustion is the primary heat source. Part of the heat of combustion is fed back to the droplet surface and the remaining part is transferred to the gas. Therefore, the rate of heat transfer from a burning droplet to the gas may be written as

$$q_g = \frac{2\pi k}{c_p} D\ (1 + 0.3\ Re^{\frac{1}{2}}\ Pr^{\frac{1}{3}})\ (H_c - h_{fg}) \cdot \ell n\ (1+B). \tag{4.18}$$

In Equation (4.18), it has been assumed that heat transfer inside the droplet is negligible. This assumption has been supported by experimental observations that the droplet is at the boiling point during most of its vapor-phase combustion period.

The heat transfer from a sodium spray to the surrounding gas is the sum of the total heat transferred from the droplets to the gas. Therefore, the total heat transfer rate from the spray to the surrounding gas may be written as

$$Q_g = \int\int q_g\ d^2N\ . \tag{4.19}$$

Similarly, Equation (4.19) can be approximated by the summation of q_g's over all the size groups and elemental volumes, namely

$$Q_g \cong \sum_i \sum_j q_g\ \Delta N_{ij}\ . \tag{4.20}$$

4.6.2 Heat Transfer to the Walls

Heat transfer from the gas to the walls of a containment cell depends on the gas and wall temperatures and gas circulation inside the cell. To determine the gas circulation flow field, one has to solve a set of conservation equations including the momentum, energy and mass transport equations. In typical sodium spray fires, the spray duration is usually very short. During this short period of time, heat transfer to the walls is insignificant in most cases. Since the gas circulation has an effect on heat transfer to the walls only, it was decided to use an empirical value for the heat transfer coefficient rather than resort to elaborate numerical schemes for solving the conservation equations.

The heat transfer rate at the walls may be expressed in terms of the heat transfer coefficient as

$$Q_w = h\, A\, (T_g - T_w). \tag{4.21}$$

The value of h for typical containment cell walls is 0.000054 cal/cm^2.s (1 Btu/ft^2 sec) as proposed by Shire.[20]

4.6.3 Heat Balance on the Gas

Heat transfer from the droplets to the cell gas will increase the gas temperature and pressure. The gas temperature inside the spray zone will be higher than that outside the spray zone. A knowledge of the average gas temperature is adequate for determining the cell pressure rise and only one average gas temperature is therefore used in the present model. Conservation of energy dictates that the increase of the internal energy of the gas must be equal to the net heat transfer to the gas. The energy equation for the cell gas may be written as

$$m_g C_{v,g} \frac{dT_g}{dt} = Q_g - Q_w \tag{4.22}$$

where m_g is the total mass of the gas inside the containment cell, $C_{v,g}$ is the specific heat of the gas at constant volume. Assuming that the gas is an ideal gas, the gas pressure may be evaluated from the ideal gas law

$$P = C\ R\ T_g\ . \tag{4.23}$$

The molar density decreases with time because of oxygen consumption. The oxygen consumption rate is computed from the droplet mass burning rate. Then the oxygen mole fraction and the molar number of oxygen are, in turn, obtained from the oxygen consumption rate at the last time step. The molar density is then computed from the total molar number of the gas mixture.

4.6.4 Heat Balance on the Walls

Heat transfer to the walls is primarily due to convective heat transfer from the gas to the walls and therefore only convective heat transfer is considered. In application to LMFBR containment cells, it is reasonable to assume that the wall temperature, T_w, is uniform and all the outer walls of the cells are thermally insulated. Under these assumptions, the energy equation for the walls becomes

$$m_w C_{v,w} \frac{dT_w}{dt} = Q_w \tag{4.24}$$

where m_w is the total mass of the walls, and $C_{v,w}$ is the specific heat of the walls.

5. THE NACOM COMPUTER PROGRAM

Using the physical models described in the previous sections, the NACOM computer program has been developed to simulate sodium spray fires postulated to occur in LMFBR containment cells. NACOM performs calculations of the single droplet and spray burning rates, heat transfer from the spray to the gas and heat transfer from the gas to the walls. The code calculates the gas and wall temperature rises, gas pressure, oxygen mole fractions, spray burning rate, etc. The program is written in the FORTRAN language for use on the CDC 7600/6600 computer system. The entire listing of the code is given in Appendix D. In this section, the code structure along with the input and output formats will be discussed.

5.1 Code Structure

The code consists of the NACOM main program, the MOTION, RATES and BALANCE subroutines, and the CD function subprogram. The main program reads input data, initializes constants, computes drop size distribution, and prints outputs. The MOTION, RATES and BALANCE subroutines perform droplet dynamic, combustion, and heat and mass transfer calculations, respectively. They are called by the main program. The CD function subprogram calculates the drag coefficient. In the following discussion, flow charts will be used to illustrate the computational procedures in each component of the code.

5.1.1 Main Program NACOM

The main program is the primary controlling program. It reads input data, initializes constants, computes drop size distribution, and prints outputs. Two options are available for reading sodium leak rate data. One is to use average sodium leak rate, where IP must be set to zero. The other is to use the variable leak rate table. There are also two output printing options. One is to

print out detailed combustion and heat transfer information and the other is to omit it completely. More detailed output discussion will be given in Section 5.3. The MOTION, RATES and BALANCE subroutines are called by the main program to perform droplet dynamic, combustion, and heat and mass transfer calculations. The flow chart for the main program is given in Fig. 8.

5.1.2 Subroutine MOTION

This subroutine is designed to perform droplet dynamic calculations. The Runge-Kutta method is used to solve the droplets' equation of motion. The velocity and distance travelled by a falling droplet are computed at discrete times t_n for eleven initial drop sizes. For convenience, a constant time step Δt is adopted, which can be adjusted by specifying a value for the time step reduction parameter, X. Because of high acceleration at the start of droplet motion, a large time step may lead to numerical instability. A time step reduction parameter of 2 is recommended as a result of compromise between accuracy and computer time. To avoid numerical instability, an asymptotic solution of the equation of droplets' motion is obtained for the initial stage of the motion. The subroutine flow chart is given in Fig. 9.

5.1.3 Function CD

The function CD uses the Reynolds number from the MOTION subroutine to calculate the drag coefficient, which is then fed back to the subroutine to compute the drag experienced by a sodium droplet falling in a gas stream. The flow chart for the function CD is given in Fig. 10.

5.1.4 Subroutine RATES

This subroutine computes the spray burning rate, heat released by the spray combustion, heat transferred to the droplets, and heat transferred to the gas from the spray. The number of drops in a specific size group, created in a Δt spray duration, is first computed using the volume fraction of the group

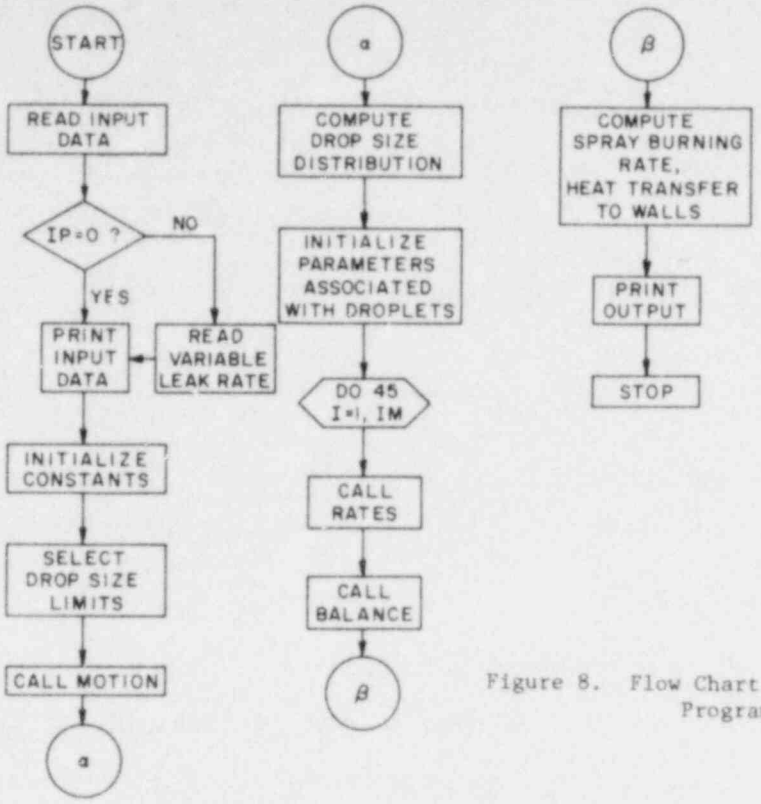

Figure 8. Flow Chart for the Main Program

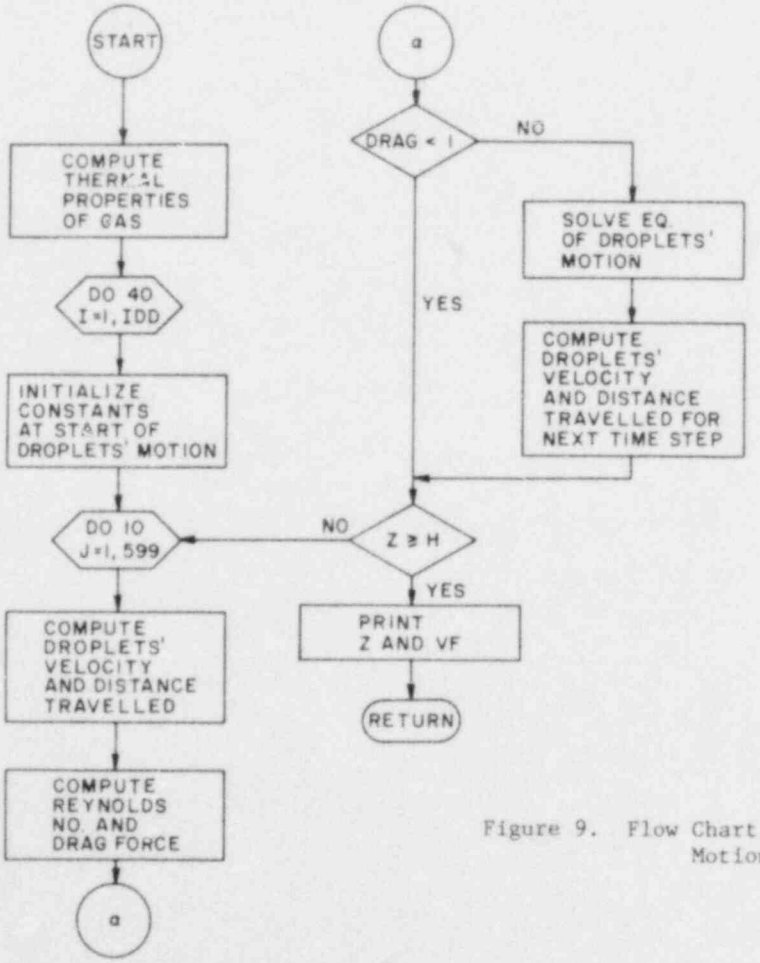

Figure 9. Flow Chart for Subroutine Motion

Figure 10. Flow Chart for Function CD

and the sodium leak rate. The average drop size, elevation, velocity, and burning rate of the group are then computed. Heat released by droplet combustion, and heat transferred to the droplet surface and the gas are, in turn, computed from the burning rate. The spray burning rate and heat transferred from the spray to the gas are simply the sum of the contributions from all the burning droplets. Finally, the drop size, number of drops and droplet temperature of each group are recomputed at the next time step. The flow chart for the subroutine RATES is given in Fig. 11.

5.1.5 Subroutine BALANCE

This subroutine does heat and mass balances. The gas and oxygen molar numbers at the next time step are computed from the amount of oxygen consumed within the present time step. The oxygen mole fraction at the next time step is then computed from the gas and oxygen molar numbers. The gas and wall temperature rises at this time step are computed from the heat transfer rates, which are input from the RATES subroutines. The flow chart for the subroutine BALANCE is shown in Fig. 12.

5.2 Input Data Format

The first card in the input deck is the title card. The title of the case run starts from the second column and less than 70 characters are allowed. The first column is set to 1 for detailed combustion and heat transfer data outputs. The following data cards are read subsequently in the main program.

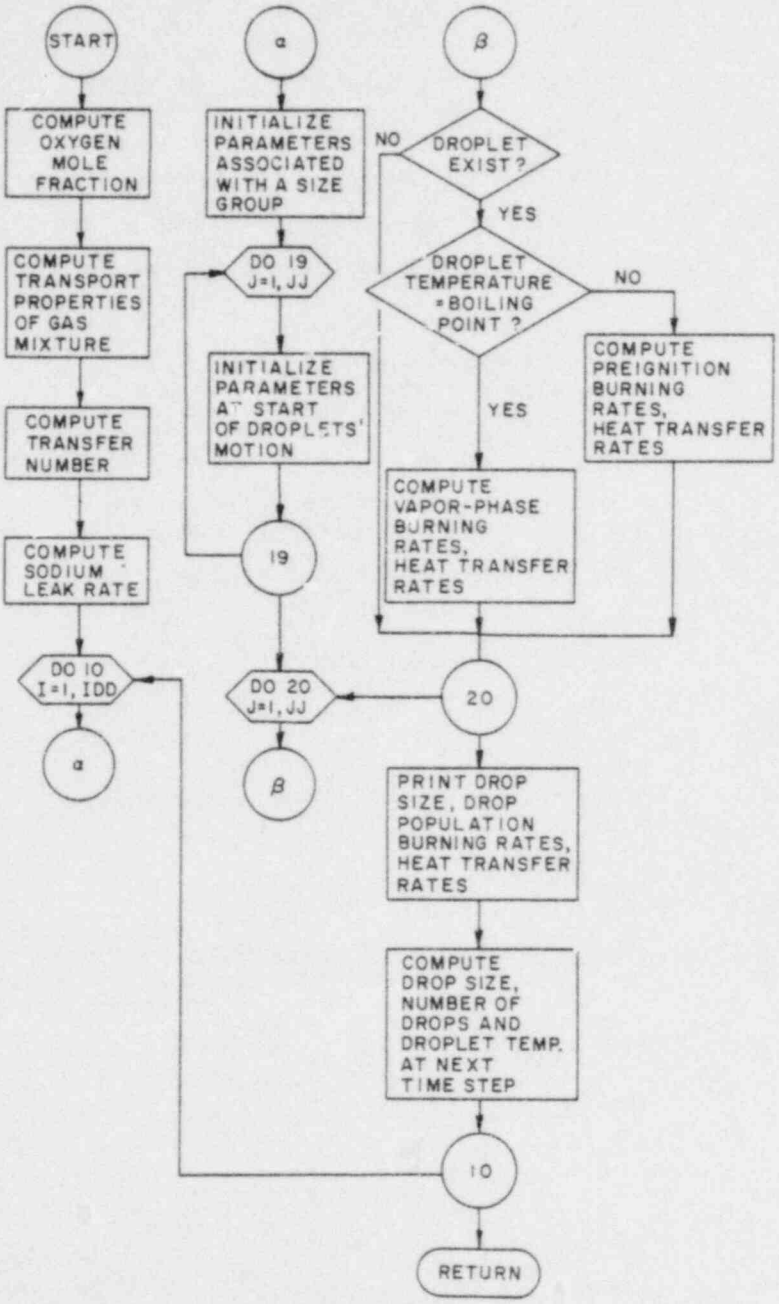

Figure 11. Flow Chart for Subroutine RATES

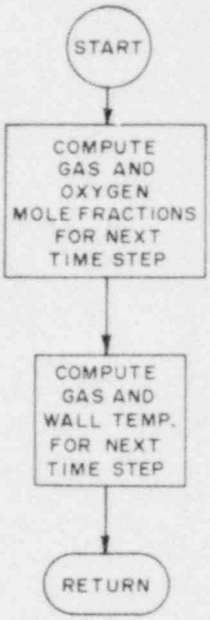

Figure 12. Flow Chart for Subroutine BALANCE

Card No.	Symbol	Columns	Format	Definition
2	ALI	1-12	F12.4	Total cell wall area (m^2)
2	H	13-24	F12.4	Cell height (m)
2	VOL	25-36	F12.4	Cell volume (m^3)
2	DME	37-48	F12.4	Volume mean droplet diameter (cm)
2	FNA	49-60	F12.4	Mean sodium leak rate (g/s)
2	TSI	61-72	F12.4	Initial sodium temperature (°C)
3	PI	1-12	F12.4	Initial cell gas pressure (atm)
3	TGI	13-24	F12.4	Initial cell gas temperature (°C)
3	YOI	25-36	F12.4	Initial oxygen mole fraction
3	TMAX	37-48	F12.4	Maximum problem time (s)
3	TEND	49-60	F12.4	Spray duration (s)
3	X	61-72	F12.4	Time step reduction parameter
4	NA2O2	1-12	F12.4	Fraction of peroxide in the reaction products
4	CPS	13-24	F12.4	Product of wall specific heat, density and thickness ($cal/cm^2°K$)
4	NPRT	25-36	I12	Print interval
4	IP	37-48	I12	Number of pairs of data used in the leak rate table (≤ 40)

Card No. 4 is followed by the following leak rate table, which is optional.

Leak Rate Table

Card No.	Time (s) (Columns 1-12)	Leak Rate (g/s) (Columns 13-24)
5	TL(1)	AML(1)
6	TL(2)	AML(2)
-----	-----	-----
-----	-----	-----
IP + 4	TL(IP)	AML(IP)

The data deck prepared according to the input data format described above will have the following outlook:

Card No.						
1	Title Card					
2	ALI	H	VOL	DME	FNA	TSI
3	PI	TGI	YOI	TMAX	TEND	X
4	NA202	CPS		NPRT	IP	
5	TL(1)	AML(1)				
6	TL(2)	AML(2)				
---	---	---				
---	---	---				
IP + 4	TL(IP)	AML(IP)				

5.3 Output Data Format

Flexibility has been considered in the code output. The print interval can be adjusted to suit specific need by adjusting the parameter NPRT. The option of printing the detailed combustion and heat transfer information is available. A sample probelm output is given in Appendix C. The printout appears in the following order:

1) The title of the case run

2) Input Listing

   All the data used for the input parameters are printed out.

3) Leak Rate Table

   The variable leak rates at discrete times are printed out.

4) Droplets' Motion

   The solutions to the equation of droplets' motion, namely, distance travelled and droplet velocity at discrete times for each size group are printed out.

5) Volume Fraction of Spray

   The volume fraction of the spray per unit diameter for each size group is printed out.

6) Detailed Combustion and Heat Transfer Information (Optional)

This option prints out the drop size, drop population, droplet temperature, Reynolds number, burning rates and heat transfer rates for each size group. Also printed out are the spray burning rate and the total heat transfer rate to the gas. The printout of these parameters is requested by assigning numeral "1" to the first column of the title card.

7) Thermal Transient

The cell pressure rise, gas temperature, wall temperature, oxygen mole fraction, spray burning rate, etc. are printed in a specified time interval.

Output Parameters

The definitions and units used for the output parameters are given below:

I = Size group number

DI = Initial diameter of size group i (cm)

TF = Droplet travelling time (s)

Z = Distance travelled by a droplet at time TF (cm)

VF = Droplet velocity at time TF (cm/s)

RD = Volume fraction of sodium spray per unit diameter, occupied by droplets in a size group (cm^{-1})

TIME = Time elapsed (s)

P = Cell pressure rise (atm)

TG = Average cell gas temperature (^{o}C)

TW = Cell wall temperature (^{o}C)

YOC = Oxygen mole fraction

BRS = Sodium spray burning rate (g/s)

SBR = Total amount of sodium burned (g)

Q = Rate of heat transfer from sodium spray to gas (cal/s)

SQ = Total amount of heat transfer from sodium spray to gas (cal)

QW = Rate of heat transfer from gas to walls (cal/s)

SQW = Total amount of heat transfer from gas to walls (cal)

MOLO = Molar number of oxygen (g-mole)

MOLG = Molar number of gas (g-mole)

SML = Total amount of sodium leakage (g)

There are also optional printout of combustion and heat transfer data. The definitions of these output parameters are given below:

D = Instantaneous droplet diameter (cm)

DN = Number of droplets in a size group

TS = Droplet temperature (^{o}C)

RE = Droplet Reynolds number

BRF = Falling droplet burning rate (g/s)

QIN = Rate of heat transfer to droplet (cal/s)

QC = Single droplet combustion heat release rate (cal/s)

QG = Rate of heat transfer from droplet to gas (cal/s)

6. VALIDATION OF THE NACOM CODE

In order to ensure that the code adequately predicts pressure and temperature rises resulting from sodium spray fires, validation of the physical models employed is required. Specifically, the models describing droplets' motion and the droplet combustion will be compared to AI experimental data.

6.1 Validation of the Model Describing Droplets' Motion

A determination of the adequacy of data on droplet velocities is crucial to the accurate determination of droplet burning rates. The droplet velocities are obtained by solving the droplets' equation of motion, namely, Equation (4.11). The single droplet burning tests[22] conducted at AI may be used for validation purposes. In these tests, the final velocities of sodium droplets with diameters ranging from 1.5 to 7 mm were measured. A case was run with NACOM to simulate the falling of sodium droplets through a distance of 14.73 m in the test vessel. Within this distance, the sodium droplets will all reach their terminal velocities. The final velocities measured in the tests are shown in Fig. 13 together with the NACOM and SPRAY-3A[2] predictions. Figure 13 shows that the final velocities predicted by both NACOM and SPRAY-3A are in good agreement with the test data for droplets larger than 4 mm. However, for small drops both NACOM and SPRAY-3A predictions of final velocities are below the test data, with the NACOM predictions a little closer to the experimental values. The discrepancy between the calculated and experimental values is due to the fact that the effect of droplet burning on the drag coefficient has not been adequately taken into account. The effect is to decrease the drag coefficient and hence increase the final velocity of the droplet.

6.2 Validation of Single Droplet Combustion Model

The single droplet combustion model is the basis for the formulation of spray combustion model becomes important in high oxygen concentrations. Therefore, it is necessary to validate the model in an air atmosphere. The single droplet burning tests[22] in air conducted at Atomics International can be used for validation purposes. In the tests, the droplets were released from the top of the test vessel, and the masses of droplets at the 14.73 meter distance from the top were measured. The diameters of the droplets used in the tests were from 1.5 to 7 mm. The NACOM calculation of the case discussed in the preceding section gives the final masses of the droplets at the 14.73 meter distance. The fraction of droplet mass burned is then computed from the initial and final masses of a droplet. The measured fraction of droplet mass burned is shown in Fig. 14 together with the NACOM and SPRAY-3A[2] predictions. The fraction of droplet mass burned decreases linearly for droplets larger than 0.3 cm. For droplet diameters less than 0.2 cm, the fraction of droplet burned is close to one that means that droplets smaller than 0.2 cm will be totally burned in the 14.73 meter travelling distance. AI attempted to correlate its data by drawing a straight line through the data points for large drops. However, the linear relationship no longer holds for droplets smaller than 0.3 cm. The NACOM prediction compares well with the experimental data while SPRAY-3A underpredicts the fraction of droplet burned. The largest discrepancy is partly due to the underprediction of droplet velocities by SPRAY-3A and partly due to the inaccurate single drop combustion model used in the code.

6.3 Code Validation by LTV Jet Tests

Atomics International has conducted a number of sodium spray dispersal tests in the Large Test Vessel, 7.62 m (25 ft) high by 3.05 m (10 ft) diameter. A 2.54 cm nozzle was centered on top of the vessel with its open end 11.43 cm

below the stainless steel impact plate as shown in Fig. 15. Sodium ejected from the nozzle at velocities 3 to 6 m/s was directed upward to impinge on the impact plate. The sodium moved radially on the plate and then rained down forming a sodium spray. The sodium spray contained droplets of mean droplet diameters ranging from 0.37 to 0.53 cm. The tests were conducted in atmospheres containing 0-21% oxygen.

To date, seven LTV Jet Tests have been performed. A summary of the LTV Jet Tests[21,22,23] is given in Table 1. It should be noted that test data obtained from Tests No. 1 and No. 2 are incomplete. In these two tests, the mean droplet diameters and resulting oxygen depletion were not recorded. To simulate these two tests with NACOM, the mean droplet diameters produced in the tests are needed as input parameters. To overcome the difficulty, estimated mean droplet diameters are used in the simulations. In Jet Tests No. 3 through No. 8, the monoxide-peroxide ratio in the reaction products was not measured. According to AI STV test results[12], in low oxygen environments, the primary reaction product is sodium monoxide. Consequently, NACOM simulation of Jet Tests No. 3 through No. 8 will assume 100% Na_2O_2 in the reaction products.

The summary of NACOM simulations of AI Jet Tests is shown in Table 2. In Table 2, the calculational results and experimental data on the maximum pressure rise, oxygen consumed, and sodium consumed for seven LTV Jet Tests are compared. It is seen that NACOM has better predictions of the maximum pressure rise than SPRAY-3A except for Jet Tests No. 3 and No. 8. In 21% oxygen, NACOM predicts higher burning rates and hence NACOM is more conservative than SPRAY-3A in terms of the pressure rise.

For more detailed information on the NACOM calculational results for the LTV Jet Tests, see Appendix B.

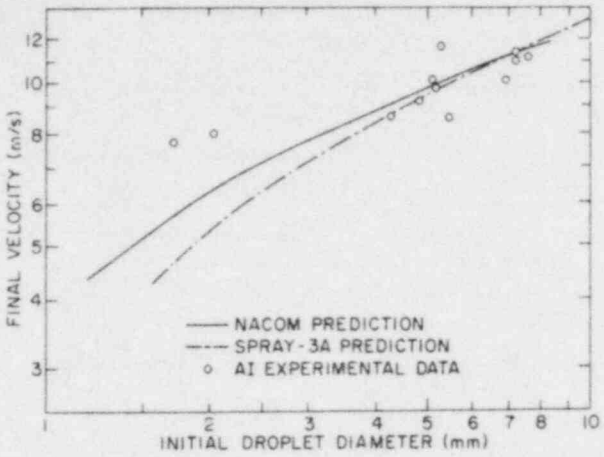

Figure 13. Comparison of Final Velocity between Predictions and AI Experimental Data

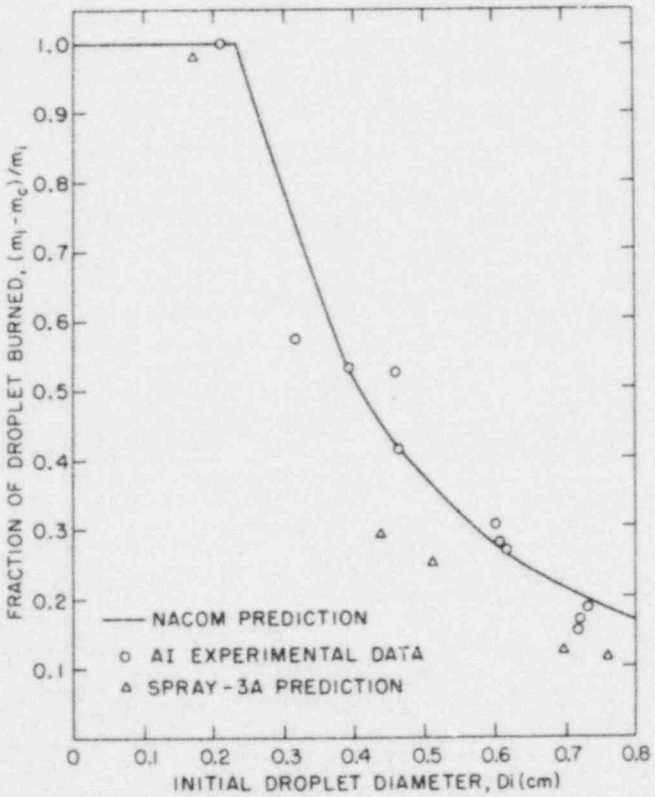

Figure 14. Comparison of Fraction of Droplet Burned between Predictions and AI Experimental Data

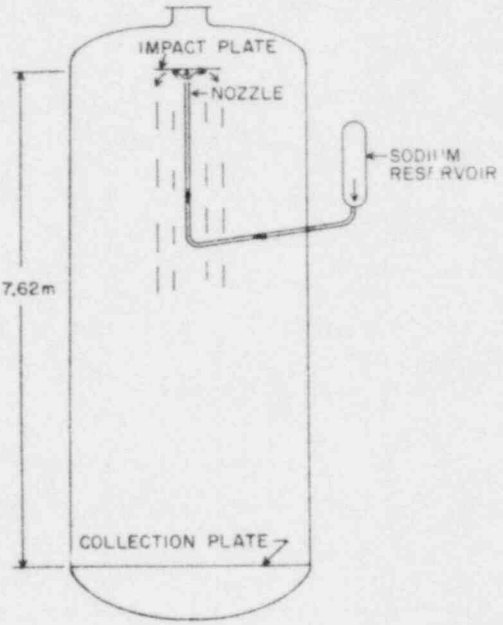

Figure 15. Sodium Jet Tests in the Large Test Vessel

Table 1. LTV Sodium Jet Test Summary

	1	2	3	4	6	7	8
Initial Oxygen Concentration (Vol %)	21	21	1.5	0	4.8	0.8	0.8
Initial Gas Temperature (°C)	23.9	23.9	20	23.9	23.9	23.9	23.9
Initial Gas Pressure (atm, gauge)			0.099	0.099	0.099	0.099	0.099
Ambient Pressure (atm)	0.97	0.97	0.97	0.97	0.97	0.97	0.97
Initial Humidity (ppm vol)	7400	8000	4400	4400	530	1100	48
Sodium Drive Pressure (atm)	17	20.7		0.83	0.83	0.83	0.83
Initial Sodium Temperature (°C)	538	538/593	532	532	529	538	538
Sodium Jet Velocity (m/s)	15.2	30.5	5.88	3.08	3.23	2.68	3.02
Sodium Release (kg)	1.72	2.40/2.45	4.08	5.62	5.58	2.36	2.72
Resulting Pressure Rise (atm)	0.22	0.8	0.053	0.039	0.29	0.046	0.033
Resulting Oxygen Depletion (vol %)			0	0	0.7	0	0
Strike Plate Temperature (°C)		1093		471	604	443	449
Sodium Drop Temperature at Floor (°C)				67	527/116	316/82	
Final Humidity (ppm vol)	3500	85			66	90	
Fallout Mean Size (μm)			0.18	0.21	0.16	0.145	0.145
Reaction Products (% Na_2O_2)	100	91-96					
Burning Efficiency	0.26	0.66					
Peak Aerosol Concentration (μm Na_2O/cc)	7.2	17.1	0.1	0.13	4.8	0.18	0.07

TABLE 2

Comparison Between Experimental Data and

Computational Results for AI Jet Tests

Test No.	Initial O_2 Concentration (mol. %)	Maximum Pressure Rise (atm.)			O_2 Consumed (mol. %)			Na Consumed (mol. %)		
		Test	NACOM	SPRAY-3A	Test	NACOM	SPRAY-3A	Test	NACOM	SPRAY-3A
J-1	21	0.22	0.23	0.20	-	0.41	0.15	26.0	40.7	31.8
J-2	21	0.80	0.68	0.60	-	1.15	0.54	66.0	85.1	70.9
J-3	1.5	0.051	0.043	0.044	0	0.02	~0	-	1.20	0.60
J-4	0.015	0.040	0.041	0.045	0	0.005	~0	-	0.009	0.48
J-6	4.8	0.29	0.11	0.10	0.7	0.12	0.04	-	4.8	2.5
J-7	0.8	0.048	0.031	0.030	0	0.008	0.003	-	0.88	1.12
J-8	0.8	0.034	0.043	0.038	0	0.012	0.004	-	0.87	1.12

7. SUMMARY AND CONCLUSIONS

The NACOM code has been developed to simulate sodium spray fires that are postulated to occur in LMFBR equipment cells. NACOM performs droplet dynamic, combustion, and heat and mass transfer calculations. The code calculates the gas pressure, gas and wall temperatures, oxygen mole fraction, spray burning rate, and heat transfer rates. The code computes the spray burning rate from the single droplet burning rates. The single droplet burning rates are, in turn, predicted by the Tsai[6] preignition oxidation model and the Spalding[15] vapor-phase combustion theory. In arriving at the spray burning rate, no adjustable parameters such as those used in SPRAY are utilized to fit spray fire experimental data. In contrast, SPRAY uses two adjustable parameters whose values are determined by curve fitting of AI experimental data. Consequently, NACOM is more reliable than SPRAY when applied to large-scale spray fires in LMFBR equipment cells and containment building.

The code has been verified by comparison with the AI single droplet burning tests. The droplet final velocities predicted by the code agree well with the AI experimental data and are somewhat better than those predicted by SPRAY-3A at small droplet diameters. The fraction of droplet mass burned predicted by NACOM for falling droplets has been found to be in good agreement with the AI experimental data while it is underpredicted by SPRAY-3A.

Further experimental verification of the code is provided by the NACOM simulation of the LTV Jet Tests. The NACOM predictions of the pressure rise are more accurate than the SPRAY-3A predictions in most cases. It appears that NACOM is more conservative than SPRAY-3A in terms of the pressure rise because SPRAY-3A underpredicts the single droplet burning rate. The code has been verified for oxygen concentrations ranging from 0 to 21%. Therefore, the code is applicable to sodium spray fires in the secondary sodium system as well as the primary sodium system of an LMFBR.

ACKNOWLEDGMENTS

The author would like to thank Dr. R. A. Bari and Dr. W. T. Pratt for helpful discussions and for providing constructive comments on the manuscript. Thanks are also due to Dr. R. J. Cerbone for reviewing the draft copy.

REFERENCES

1. P.R. Shire, "SPRAY Code User's Report," HEDL-TME 76-94, March 1977.

2. P.R. Shire, "SPRAY Code Modification and Verification with Experimental Test Results, SPRAY-3A Version," HEDL-TI-75293, February 1978.

3. M.P. Heisler and K. Mori, "SOMIX-1 Users Manual for the LBL CDC 7600 Computer," N707TI130045, Atomics International, June 1976.

4. T.S. Krolikowski, "Violently Sprayed Sodium-Air Reaction in an Enclosed Volume," ANL-7472, Argonne National Laboratory, September 1968.

5. J.R. Richard, R. Delbourgo, and P. Laffitte, "Spontaneous Ignition and Combustion of Sodium Droplets in Various Oxidizing Atmospheres at Atmospheric Pressure," Twelfth Symposium (International) on Combustion, pp. 39-48, 1969.

6. S.S. Tsai, "Surface Oxidation Process Prior to Ignition of a Sodium Droplet," Trans. Am. Nucl. Soc., 27, 524, 1977.

7. F.L. Mangold and R.A. Tidball, "Sodium Fire Studies," NP-3812, April 1952.

8. E. Hines and J.K. Kelley, "Determination of the Maximum Pressures Attained During the Reaction of Sodium with Air in Closed Systems," Detroit Edison Report 55-C-80, February 1956.

9. J.R. Humphreys Jr., "Sodium-Air Reactions as They Pertain to Reactor Safety and Containment," Proceedings of Second International Conference on Peaceful Uses of Atomic Energy, Geneva, Vol. 22, p. 177, 1958.

10. J.D. Gracie and J.J. Droher, "A Study of Sodium Fires," NAA-SR-4383, Atomics International, October 1960.

11. I. Charak and F.A. Smith, "Preliminary Evaluation of a Technique to Study Expulsion of Sodium into Air," Proceedings of Conference on Safety, Fuel and Core Design in Large Fast Power Reactors, ANL-7120, Argonne National Laboratory, p. 868, October 1965.

12. "Quarterly Technical Progress Report, LMFBR Safety Programs, January-March 1971," AI-AEC-12992, Atomics International, May 1971.

13. "Quarterly Technical Progress Report, LMFBR Safety Programs, January-March 1972," AI-AEC-13026, Atomics International, May 1972.

14. "Quarterly Technical Progress Report, Nuclear Safety, Characterization of Sodium Fires and Fast Reactor Fission Products, July-September 1975," AI-ERDA-13161, Atomics International, November 1975.

15. D.B. Spalding, "Some Fundamentals of Combustion," Butterworths, London, England, 1955.

16. "Annual Technical Progress Report, LMFBR Safety Programs, GFY 1971," AI-AEC-13006, Atomics International, September 1971.

17. W.E. Ranz and W.R. Marshall, Jr., "Evaporation from Drops, Part II," Chem. Eng. Progr., Vol. 48, No. 4, pp. 173-180, April 1952.

18. G.A. Agoston, H. Wise and W.A. Rosser, "Dynamic Factors Affecting the Combustion of Liquid Spheres 6th Symposium (Int.) on Combustion, Reinhold, New York, p. 708, 1957.

19. E. Mayer, "Vaporization Rate Limited Combustion in Bipropellant Rocket Chambers," ARS Journal, July 1959.

20. P.R. Shire, "A Combustion Model for Hypothetical Sodium Spray Fire Within Containment for an LMFBR," M.S. Thesis, University of Washington, 1972.

21. L. Baurmash, et al., "Test Report - Sodium Fires Experiment, Jet Tests No. 6, 7 and 8," TR-707-130-002, Atomics International, May 1972.

22. R.P. Johnson, et al., "Test Report for the Sodium Drop Burning and Velocity Tests for SOMIX," N-707-TR-130022, Atomics International, September 1977.

23. L. Baurmash, et al., "Test Report - Sodium Fires Experiment, Jet Tests No. 3 and 4," TR-707-130-001, Atomics International, March 1972.

24. L. Baurmash, et al., "Summary Report for Laboratory Experiments on Sodium Fires," TR-707-130-007, Atomics International, August 1973.

APPENDIX A

THE PHYSICAL PROPERTIES

The transport properties of the gas mixture surrounding a sodium droplet vary substantially with the gas composition and the gas temperature. An accurate determination of the properties is difficult because the gas composition and the gas temperature vary considerably from the droplet surface to the burning zone and from the burning zone to the surroundings. Therefore, mean values of the transport properties must be used. In the code, the arithmetic mean of the droplet temperature and the gas temperature is used to compute the transport properties of the gas mixture. The variation of the transport properties with the gas composition is less pronounced. It is a good approximation to assume that the gas is 100% N_2 in the evaluation of the transport properties since the gas mixture is predominantly nitrogen.

For the droplets' motion, however, the oncoming properties of the gas stream are used, which were found to be in better agreement with experimental data.

In the code, the physical properties are considered as functions of temperature and pressure only. The following formulas are used to compute the physical properties. In the formulas, the unit of temperature T is $^{\circ}K$ and the unit of pressure P is atmosphere.

Nitrogen

Specific heat (cal/g·K)

$$C_p = 0.2316 + 4.61 \times 10^{-5} T$$

Absolute viscosity (g/cm·s)

$$\mu = 4.2 \times 10^{-6} T^{0.56}$$

Thermal conductivity (cal/cm·s·K)

$$k = 1.05 \times 10^{-6} T^{0.71852}$$

Mass Transfer

N_2-O_2 binary diffusion coefficient (cm^2/s)

$$D = 1.849 \times 10^{-5} \frac{T^{1.645}}{P}$$

Product of molar density and binary diffusion coefficient (g-mole/cm·s)

$$CD = 2.25 \times 10^{-7} T^{0.645}$$

Sodium

Density of the liquid (g/cm^3)

$$\rho = 0.949 - 2.23 \times 10^{-4}(T-273) - 1.75 \times 10^{-8} (T-273)^2$$

Specific heat of the liquid (cal/g·K)

$$C_p = 0.34324 - 1.3868 \times 10^{-4} (T-273) + 1.1044 \times 10^{-7} (T-273)^2$$

The heat of combustion H_c and the stoichiometric ratio i depend on the composition of the reaction products. When the fraction of Na_2O_2 present in the reaction products, f, is known, the fraction of unit mass of sodium that reacts with oxygen to form Na_2O_2 is

$$S = 1.3478f/(1.6957 - 0.3479f)$$

The heat of combustion may be expressed in terms of S as

$$H_c = 2195 (1-S) + 2500 S \qquad \text{(cal/g)}$$

and the stoichiometric ratio may be written as

$$i = \frac{S}{1.4375} + \frac{1-S}{2.875} \qquad \left(\frac{\text{g of } O_2}{\text{g of Na}} \right)$$

APPENDIX B

NACOM SIMULATION OF LTV JET TESTS

B.1 Jet Test No. 1

In this test, 1.72 Kg of sodium at 538°C were injected at 15.2 m/s into a 21% oxygen atmosphere. Since the mean droplet diameter was not measured, a mean droplet diameter of 2 mm, estimated by Shi [2] using a correlation of jet velocity and drop size, was used in the NACOM simulation of the test.

The NACOM calculational results for the test are shown in Figs. 16 and 17. It is seen from Fig. 16 that a maximum pressure rise of 0.23 atm is reached at 2.2 seconds. The NACOM prediction of the maximum pressure rise is about 5% higher than the experimental value, while the SPRAY-3A prediction is about 9% lower. The NACOM-calculated maximum gas temperature is 88°C. The NACOM-predicted burning efficiency (amount of sodium consumed/amount of sodium leaked) is 41% which is about 57% higher than the experimental value. The discrepancy may be due to the inaccurate estimate of the mean droplet diameter.

B.2 Jet Test No. 2

In this test, 2.4 kg of sodium at 538°C were injected at 30.5 m/s into a 21% oxygen atmosphere. An estimated mean droplet diameter of 1 mm[2] was used in the NACOM analysis of this test.

The calculated cell pressure rise and gas temperature are shown in Figs. 18 and 19, respectively. The calculated maximum pressure rise is 0.68 atm at 2.2 seconds as compared to the experimentally observed maximum pressure rise of 0.8 atm at 2 seconds. The calculated maximum gas temperature is 214°C. A burning efficiency of 85% is predicted, which is about 29% higher than the experimental result. The SPRAY-3A predicts a lower burning efficiency and hence a lower pressure rise. It appears that NACOM is more conservative than SPRAY-3A in an air atmosphere, because NACOM has a higher single droplet burning rate.

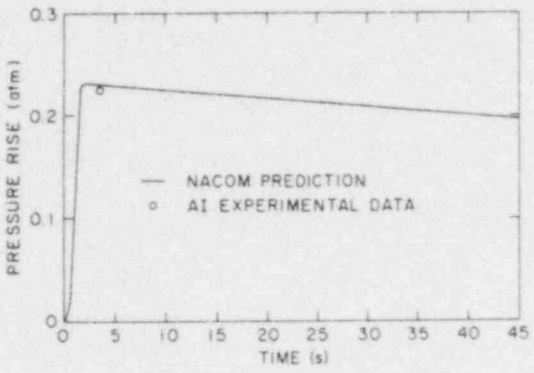

Figure 16. NACOM Prediction of Pressure History for LTV Jet Test No. 1

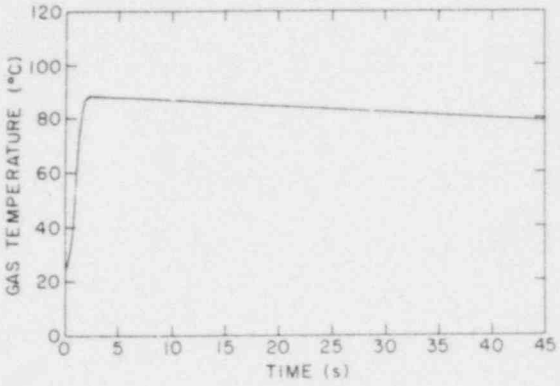

Figure 17. NACOM Prediction of Gas Temperature History for LTV Jet Test No. 1

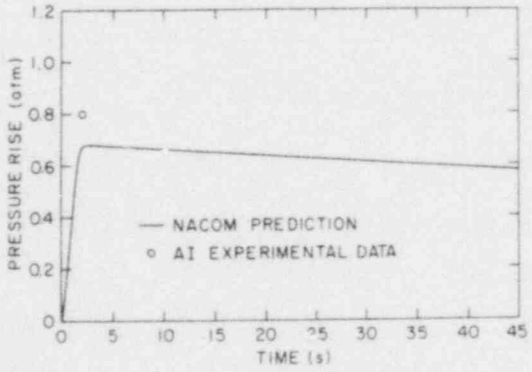

Figure 18. NACOM Prediction of Pressure History for LTV Jet Test No. 2

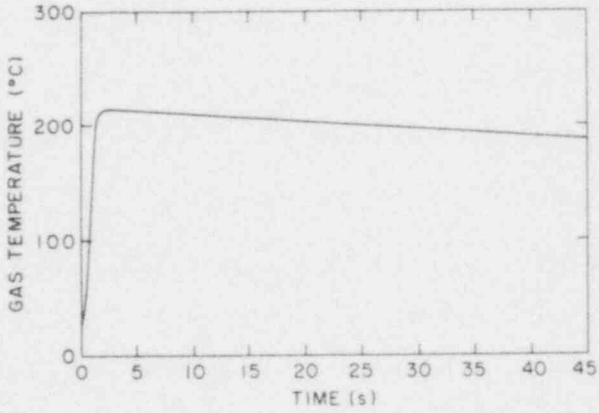

Figure 19. NACOM Prediction of Gas Temperature History for LTV Jet Test No. 2

B.3 Jet Test No. 3

4.08 kg of sodium at 532°C were injected into a 1.5% oxygen atmosphere at 5.88 m/s over a 2.7 second period. The measured mean droplet diameter was 0.457 cm. The pressure rise and gas temperature predicted by NACOM are shown in Figs. 20 and 21, respectively. The pressure reaches its peak of 0.043 atm at 4 seconds. The maximum pressure rise predicted by NACOM is about 16% lower than the observed value and is about the same as that predicted by SPRAY-3A. The low pressure rise predicted is mainly due to high humidity (0.8%) in the atmosphere since the water vapor is almost consumed after the test. The NACOM prediction of the maximum gas temperature is 30°C, compared with the experimental value of 33°C.

B.4 Jet Test No. 4

In this test, 5.62 kg of sodium at 532°C were injected into a zero oxygen atmosphere at 3.08m/s over a 5.7 second period. The measured mean droplet diameter was 0.533 cm. The NACOM calculational results for this test are shown in Figs. 22 and 23. The maximum pressure rise predicted by NACOM is 0.041 atm reached at 6.6 seconds, compared with the measured value and SPRAY-3A prediction of 0.04 atm and 0.045 atm, respectively. This shows that the heat transfer models used in NACOM are better than those used in SPRAY-3A. The NACOM prediction of the maximum gas temperature is 35°C, which is the same as the experimental value.

B.5 Jet Test No. 6

In this test, 5.58 kg of sodium at 529°C were injected into a 4.8% O_2 atmosphere at 3.23 m/s over a three second period. The measured mean droplet diameter was 0.406 cm. The NACOM calculational results for this test are shown in Figs. 24 and 25. The maximum pressure rise predicted by NACOM is 0.11 atm reached at 6.8 seconds, compared with the measured value of 0.29 atm and SPRAY-3A prediction of 0.10 atm. The large discrepancy between experiment and predictions

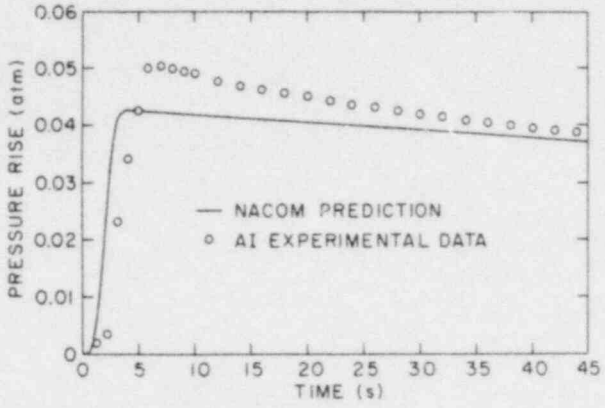

Figure 20. NACOM Prediction of Pressure History for LTV Jet Test No. 3

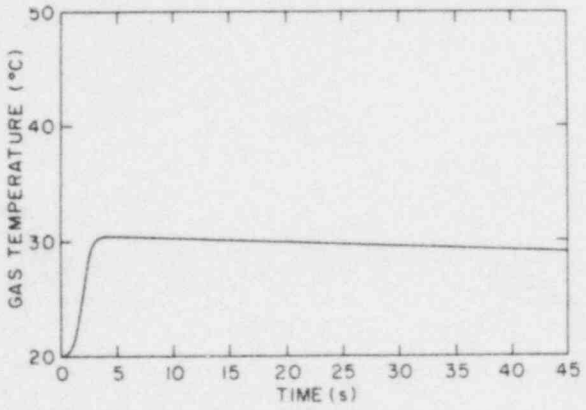

Figure 21. NACOM Prediction of Gas Temperature History for LTV Jet Test No. 3

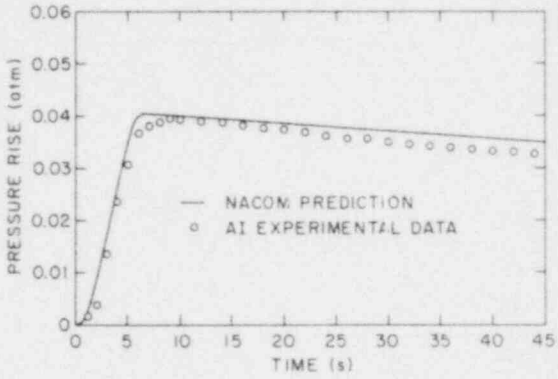

Figure 22. NACOM Prediction of Pressure History for LTV Jet Test No. 4

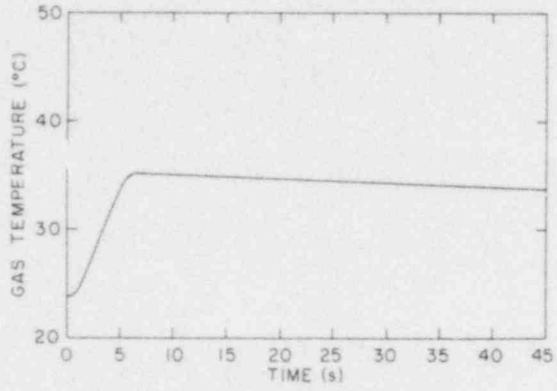

Figure 23. NACOM Prediction of Gas Temperature History for LTV Jet Test No. 4

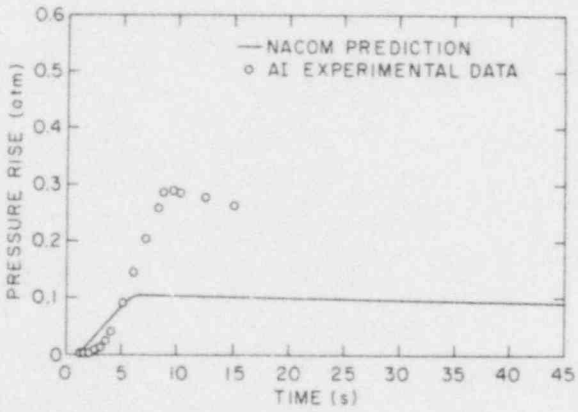

Figure 24. NACOM Prediction of Pressure History for LTV Jet Test No. 6

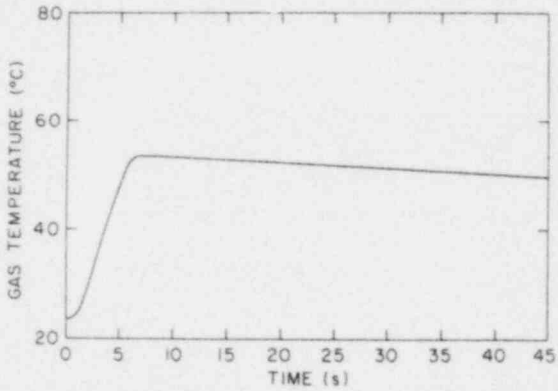

Figure 25. NACOM Prediction of Gas Temperature History for LTV Jet Test No. 6

is because the effect of water vapor on sodium burning is very pronounced in this test. The effect has not been considered in the present version of the NACOM code. The sodium injection resulted in 0.7% oxygen consumption, compared with the NACOM and SPRAY-3A predictions of 0.12% and 0.04%, respectively. The maximum gas temperature predicted by NACOM is 54°C, compared with the experimental value of 103° C.

B.6 Jet Test No. 7

In this test, 2.36 kg of sodium at 538°C were injected into a 0.8% O_2 atmosphere at 2.68 m/s over a 3.3 second period. The measured mean droplet diameter was 0.356 cm. The NACOM calculational results for this test are shown in Figs. 26 and 27. The maximum pressure rise predicted by NACOM is 0.03 atm which is about 38% lower than the experimental value. Again, in this test water vapor plays an important role in increasing sodium burning rate and hence increasing pressure rise. The maximum gas temperature predicted by NACOM is 32°C, compared with the experimental value of 37°C.

B.7 Jet Test No. 8

In this test, 2.72 kg of sodium at 538°C were injected into a 0.8% O_2 atmosphere at 3.02 m/s over a 3.3 second period. The measured mean droplet diameter was 0.369 cm. The NACOM calculational results for this test are shown in Figs. 28 and 29. NACOM predicts a maximum pressure rise of 0.043 atm at 4.8 seconds while SPRAY-3A predicts a maximum pressure rise of 0.038 atm. In comparison, the measured maximum pressure rise is 0.034 atm. This test is essentially the same as Jet Test No. 7 except that the amount of sodium injected is higher and humidity is lower in this test. The lower humidity leads to lower pressure rise observed in this test even though the amount of sodium injected is higher in this test. The maximum gas temperature predicted by NACOM is 36°C, which is 12% higher than the experimental value.

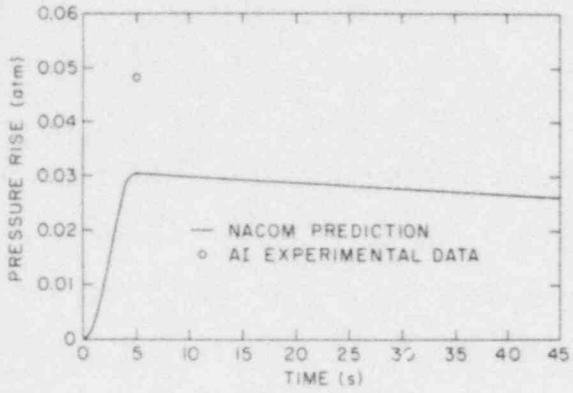

Figure 26. NACOM Prediction of Pressure History for LTV Jet Test No. 7

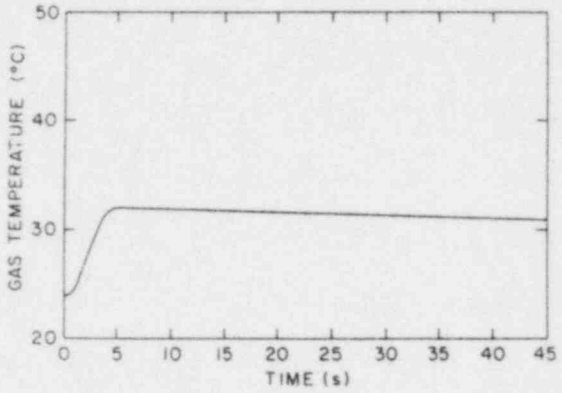

Figure 27. NACOM Prediction of Gas Temperature History for LTV Jet Test No. 7

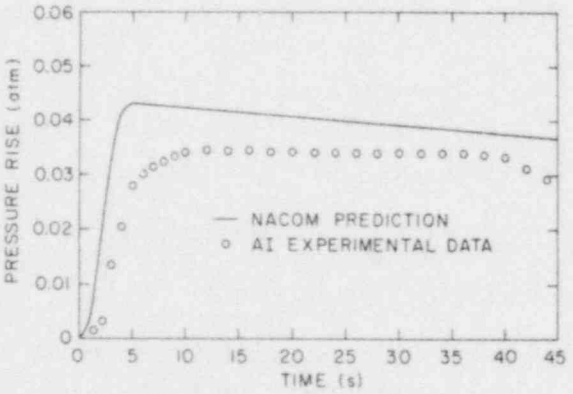

Figure 28. NACOM Prediction of Pressure History for LTV Jet Test No. 8

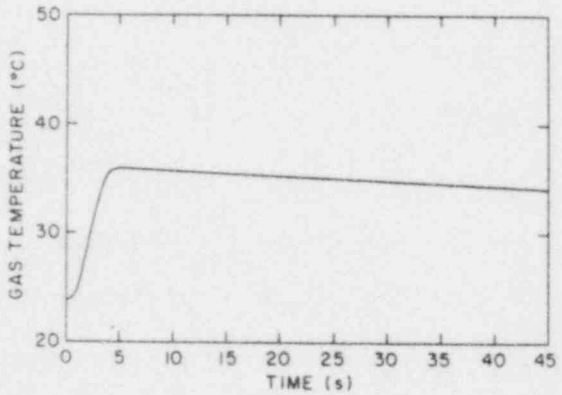

Figure 29. NACOM Prediction of Gas Temperature History for LTV Jet Test No. 8

APPENDIX C

SAMPLE PROBLEM

A detailed description of the code structure, and the input and output formats is given in the previous sections. For illustrative purposes, a sample problem will be solved by use of the NACOM code. The problem selected for these purposes is AI Jet Test No. 8[21] in the Large Test Vessel (LTV). In this test, 2.7 kg of 538°C sodium were injected into the LTV filled with 0.8% O_2. The LTV is a right circular cylinder, 9.14 m long and 3.05 m in diameter. The measured volume mean diameter of the droplets is 0.369 cm.

The input data deck for this sample problem is given as follows.

```
0                    AI JET TEST NO.8-SODIUM SPRAY IN LTV.

93.5863        7.62          62.2971        C  .9          824.6        537.8
1.07           23.9          0.008          C.             3.3          2.
0.             0.586                  25                  8
0.             0.
0.5            1556.8
1.0            1354.3
1.5            1183.4
2.0            1107.5
2.5            1069.5
3.0            601.2
3.4            0.
```

The first column in the title card has been set to zero for the option of omitting the detailed combustion and heat transfer outputs. These outputs can be obtained by setting the first column to one. The code outputs for this sample problem are given on the following page. The major output parameters of interest are the pressure rise, gas and wall temperatures, oxygen mole fraction, and spray burning rate. The histories of these output parameters are shown in Fig. 28 through 32.

AI JET TEST NO.8 - SODIUM SPRAY IN LTV.

INPUT LISTING

ALI= .9359E+02 H= .7620E+01 VOL= .6230E+02 DME= .3690E+00 ENA= .8246E+03 TSI= .537AE+03

PI= .1070E+01 TGI= .2390E+02 YOI= .8000E-02 TMAX= .4600E+02 TEND= .3300E+01 X= .2000E+01

NA2O2=0. CPS= .5860E+00 NPRT= 250 IP= 8

TIME(S)	FLOW RATE(G/S)
0.	0.
.5000E+00	.1557E+04
.1000E+01	.1354E+04
.1500E+01	.1163E+04
.2000E+01	.1108E+04
.2500E+01	.1070E+04
.3000E+01	.6012E+03
.3400E+01	0.

I= 1 DI= .7947E-01

TF	0.	.2000E-01	.4000E-01	.6000E-01	.8000E-01	.1000E+00	.1200E+00	.1400E+00	.1600E+00	.1800E+00
TF	.2000E+00	.2200E+00	.2400E+00	.2600E+00	.2800E+00	.3000E+00	.3200E+00	.3400E+00	.3600E+00	.3800E+00
TF	.4000E+00	.4200E+00	.4400E+00	.4600E+00	.4800E+00	.5000E+00	.5200E+00	.5400E+00	.5600E+00	.5800E+00
TF	.6000E+00	.6200E+00	.6400E+00	.6600E+00	.6800E+00	.7000E+00	.7200E+00	.7400E+00	.7600E+00	.7800E+00
TF	.8000E+00	.8200E+00	.8400E+00	.8600E+00	.8800E+00	.9000E+00	.9200E+00	.9400E+00	.9600E+00	.9800E+00
TF	.1000E+01	.1020E+01	.1040E+01	.1060E+01	.1080E+01	.1100E+01	.1120E+01	.1140E+01	.1160E+01	.1180E+01
TF	.1200E+01	.1220E+01	.1240E+01	.1260E+01	.1280E+01	.1300E+01	.1320E+01	.1340E+01	.1360E+01	.1380E+01
TF	.1400E+01	.1420E+01	.1440E+01	.1460E+01	.1480E+01	.1500E+01	.1520E+01	.1540E+01	.1560E+01	.1580E+01
TF	.1600E+01	.1620E+01	.1640E+01	.1660E+01	.1680E+01	.1700E+01	.1720E+01	.1740E+01	.1760E+01	.1780E+01
TF	.1800E+01	.1820E+01	.1840E+01	.1860E+01	.1880E+01	.1900E+01	.1920E+01	.1940E+01	.1960E+01	.1980E+01
TF	.2000E+01	.2020E+01	.2040E+01	.2060E+01	.2080E+01	.2100E+01	.2120E+01	.2140E+01	.2160E+01	.2180E+01
TF	.2200E+01	.2220E+01	.2240E+01	.2260E+01	.2280E+01	.2300E+01	.2320E+01	.2340E+01	.2360E+01	.2380E+01
TF	.2400E+01	.2420E+01	.2440E+01	.2460E+01	.2480E+01	.2500E+01	.2520E+01	.2540E+01	.2560E+01	.2580E+01
TF	.2600E+01	.2620E+01	.2640E+01	.2660E+01	.2680E+01	.2700E+01	.2720E+01	.2740E+01	.2760E+01	.2780E+01
TF	.2800E+01	.2820E+01	.2840E+01	.2860E+01	.2880E+01	.2900E+01	.2920E+01	.2940E+01	.2960E+01	.2980E+01
TF	.3000E+01									

Z	0.	.2000E-09	.3879E+00	.1151E+01	.2273E+01	.3735E+01	.5518E+01	.7602E+01	.9968E+01	.1260E+02
Z	.1547E+02	.1857E+02	.2187E+02	.2537E+02	.2905E+02	.3288E+02	.3687E+02	.4099E+02	.4524E+02	.4960E+02
Z	.5407E+02	.5863E+02	.6328E+02	.6801E+02	.7281E+02	.7767E+02	.8260E+02	.8758E+02	.9261E+02	.9768E+02
Z	.1028E+03	.1079E+03	.1131E+03	.1183E+03	.1236E+03	.1289E+03	.1341E+03	.1395E+03	.1448E+03	.1501E+03
Z	.1555E+03	.1609E+03	.1663E+03	.1716E+03	.1771E+03	.1825E+03	.1879E+03	.1933E+03	.1988E+03	.2042E+03
Z	.2097E+03	.2151E+03	.2206E+03	.2261E+03	.2315E+03	.2370E+03	.2425E+03	.2480E+03	.2535E+03	.2589E+03
Z	.2644E+03	.2699E+03	.2754E+03	.2809E+03	.2864E+03	.2919E+03	.2974E+03	.3029E+03	.3084E+03	.3139E+03
Z	.3194E+03	.3249E+03	.3304E+03	.3359E+03	.3414E+03	.3469E+03	.3524E+03	.3579E+03	.3634E+03	.3689E+03
Z	.3744E+03	.3799E+03	.3854E+03	.3909E+03	.3964E+03	.4020E+03	.4075E+03	.4130E+03	.4185E+03	.4240E+03
Z	.4295E+03	.4350E+03	.4405E+03	.4460E+03	.4515E+03	.4570E+03	.4625E+03	.4680E+03	.4735E+03	.4790E+03
Z	.4846E+03	.4901E+03	.4956E+03	.5011E+03	.5066E+03	.5121E+03	.5176E+03	.5231E+03	.5286E+03	.5341E+03
Z	.5396E+03	.5451E+03	.5506E+03	.5562E+03	.5617E+03	.5672E+03	.5727E+03	.5782E+03	.5837E+03	.5892E+03
Z	.5947E+03	.6002E+03	.6057E+03	.6112E+03	.6167E+03	.6222E+03	.6278E+03	.6333E+03	.6388E+03	.6443E+03
Z	.6498E+03	.6553E+03	.6608E+03	.6663E+03	.6718E+03	.6773E+03	.6828E+03	.6883E+03	.6939E+03	.6994E+03
Z	.7049E+03	.7104E+03	.7159E+03	.7214E+03	.7269E+03	.7324E+03	.7379E+03	.7434E+03	.7489E+03	.7544E+03
Z	.7599E+03									

```
VF    .1000E-07  .1939E+02  .3815E+02  .5609E+02  .7311E+02  .8916E+02  .1042E+03  .1183E+03  .1314E+03  .1436E+03
VF    .1549E+03  .1653E+03  .1749E+03  .1838E+03  .1919E+03  .1993E+03  .2062E+03  .2124E+03  .2181E+03  .2233E+03
VF    .2281E+03  .2324E+03  .2364E+03  .2400E+03  .2433E+03  .2463E+03  .2490E+03  .2514E+03  .2537E+03  .2557E+03
VF    .2575E+03  .2592E+03  .2607E+03  .2621E+03  .2634E+03  .2645E+03  .2655E+03  .2664E+03  .2673E+03  .2681E+03
VF    .2687E+03  .2694E+03  .2699E+03  .2705E+03  .2709E+03  .2713E+03  .2717E+03  .2721E+03  .2724E+03  .2727E+03
VF    .2729E+03  .2732E+03  .2734E+03  .2736E+03  .2737E+03  .2739E+03  .2740E+03  .2742E+03  .2743E+03  .2744E+03
VF    .2745E+03  .2746E+03  .2746E+03  .2747E+03  .2748E+03  .2748E+03  .2749E+03  .2749E+03  .2750E+03  .2750E+03
VF    .2751E+03  .2751E+03  .2751E+03  .2751E+03  .2752E+03  .2752E+03  .2752E+03  .2752E+03  .2752E+03  .2753E+03
VF    .2753E+03  .2753E+03  .2753E+03  .2753E+03  .2753E+03  .2753E+03  .2753E+03  .2753E+03  .2753E+03  .2753E+03
VF    .2753E+03  .2754E+03  .2754E+03  .2754E+03  .2754E+03  .2754E+03  .2754E+03  .2754E+03  .2754E+03  .2754E+03
VF    .2754E+03  .2754E+03  .2754E+03  .2754E+03  .2754E+03  .2754E+03  .2754E+03  .2754E+03  .2754E+03  .2754E+03
VF    .2754E+03  .2754E+03  .2754E+03  .2754E+03  .2754E+03  .2754E+03  .2754E+03  .2754E+03  .2754E+03  .2754E+03
VF    .2754E+03  .2754E+03  .2754E+03  .2754E+03  .2754E+03  .2754E+03  .2754E+03  .2754E+03  .2754E+03  .2754E+03
VF    .2754E+03  .2754E+03  .2754E+03  .2754E+03  .2754E+03  .2754E+03  .2754E+03  .2754E+03  .2754E+03  .2754E+03
VF    .2754E+03  .2754E+03  .2754E+03  .2754E+03  .2754E+03  .2754E+03  .2754E+03  .2754E+03  .2754E+03  .2754E+03
VF    .2754E+03

I=  2    DI= .2191E+00

TF    0.         .2000E-01  .4000E-01  .6000E-01  .8000E-01  .1000E+00  .1200E+00  .1400E+00  .1600E+00  .1800E+00
TF    .2000E+00  .2200E+00  .2400E+00  .2600E+00  .2800E+00  .3000E+00  .3200E+00  .3400E+00  .3600E+00  .3800E+00
TF    .4000E+00  .4200E+00  .4400E+00  .4600E+00  .4800E+00  .5000E+00  .5200E+00  .5400E+00  .5600E+00  .5800E+00
TF    .6000E+00  .6200E+00  .6400E+00  .6600E+00  .6800E+00  .7000E+00  .7200E+00  .7400E+00  .7600E+00  .7800E+00
TF    .8000E+00  .8200E+00  .8400E+00  .8600E+00  .8800E+00  .9000E+00  .9200E+00  .9400E+00  .9600E+00  .9800E+00
TF    .1000E+01  .1020E+01  .1040E+01  .1060E+01  .1080E+01  .1100E+01  .1120E+01  .1140E+01  .1160E+01  .1180E+01
TF    .1200E+01  .1220E+01  .1240E+01  .1260E+01  .1280E+01  .1300E+01  .1320E+01  .1340E+01  .1360E+01  .1380E+01
TF    .1400E+01  .1420E+01  .1440E+01  .1460E+01  .1480E+01  .1500E+01  .1520E+01  .1540E+01  .1560E+01  .1580E+01
TF    .1600E+01  .1620E+01

Z     0.         .2000E-09  .3912E+00  .1171E+01  .2336E+01  .3882E+01  .5805E+01  .8099E+01  .1076E+02  .1378E+02
Z     .1716E+02  .2089E+02  .2496E+02  .2937E+02  .3412E+02  .3919E+02  .4458E+02  .5028E+02  .5629E+02  .6260E+02
Z     .6921E+02  .7611E+02  .8328E+02  .9073E+02  .9844E+02  .1064E+03  .1146E+03  .1230E+03  .1317E+03  .1406E+03
Z     .1497E+03  .1590E+03  .1684E+03  .1781E+03  .1879E+03  .1979E+03  .2081E+03  .2184E+03  .2289E+03  .2395E+03
Z     .2503E+03  .2611E+03  .2721E+03  .2832E+03  .2944E+03  .3057E+03  .3171E+03  .3286E+03  .3402E+03  .3519E+03
Z     .3637E+03  .3755E+03  .3874E+03  .3994E+03  .4114E+03  .4235E+03  .4357E+03  .4479E+03  .4602E+03  .4725E+03
Z     .4848E+03  .4972E+03  .5097E+03  .5221E+03  .5347E+03  .5472E+03  .5598E+03  .5724E+03  .5851E+03  .5977E+03
Z     .6104E+03  .6231E+03  .6359E+03  .6487E+03  .6614E+03  .6743E+03  .6871E+03  .6999E+03  .7128E+03  .7257E+03
Z     .7385E+03  .7515E+03

VF    .1000E-07  .1956E+02  .3899E+02  .5825E+02  .7730E+02  .9613E+02  .1147E+03  .1331E+03  .1511E+03  .1689E+03
VF    .1864E+03  .2036E+03  .2206E+03  .2372E+03  .2535E+03  .2695E+03  .2852E+03  .3006E+03  .3156E+03  .3304E+03
VF    .3448E+03  .3588E+03  .3723E+03  .3854E+03  .3980E+03  .4102E+03  .4219E+03  .4332E+03  .4440E+03  .4544E+03
VF    .4644E+03  .4740E+03  .4832E+03  .4920E+03  .5004E+03  .5084E+03  .5161E+03  .5234E+03  .5304E+03  .5370E+03
VF    .5433E+03  .5493E+03  .5551E+03  .5605E+03  .5657E+03  .5706E+03  .5753E+03  .5797E+03  .5839E+03  .5879E+03
VF    .5917E+03  .5953E+03  .5986E+03  .6019E+03  .6049E+03  .6078E+03  .6105E+03  .6131E+03  .6155E+03  .6178E+03
VF    .6200E+03  .6220E+03  .6240E+03  .6258E+03  .6276E+03  .6292E+03  .6308E+03  .6322E+03  .6336E+03  .6349E+03
VF    .6361E+03  .6373E+03  .6384E+03  .6394E+03  .6404E+03  .6413E+03  .6422E+03  .6430E+03  .6438E+03  .6445E+03
VF    .6452E+03  .6458E+03

I=  3    DI= .3588E+00

TF    0.         .2000E-01  .4000E-01  .6000E-01  .8000E-01  .1000E+00  .1200E+00  .1400E+00  .1600E+00  .1800E+00
TF    .2000E+00  .2200E+00  .2400E+00  .2600E+00  .2800E+00  .3000E+00  .3200E+00  .3400E+00  .3600E+00  .3800E+00
TF    .4000E+00  .4200E+00  .4400E+00  .4600E+00  .4800E+00  .5000E+00  .5200E+00  .5400E+00  .5600E+00  .5800E+00
TF    .6000E+00  .6200E+00  .6400E+00  .6600E+00  .6800E+00  .7000E+00  .7200E+00  .7400E+00  .7600E+00  .7800E+00
TF    .8000E+00  .8200E+00  .8400E+00  .8600E+00  .8800E+00  .9000E+00  .9200E+00  .9400E+00  .9600E+00  .9800E+00
TF    .1000E+01  .1020E+01  .1040E+01  .1060E+01  .1080E+01  .1100E+01  .1120E+01  .1140E+01  .1160E+01  .1180E+01
TF    .1200E+01  .1220E+01  .1240E+01  .1260E+01  .1280E+01  .1300E+01  .1320E+01  .1340E+01  .1360E+01  .1380E+01
TF    .1400E+01  .1420E+01  .1440E+01  .1460E+01  .1480E+01
```

Z	0.	.2000E-09	.3916E+00	.1174E+01	.2345E+01	.3903E+01	.5846E+01	.8171E+01	.1088E+02	.1396E+02
Z	.1742E+02	.2125E+02	.2545E+02	.3002E+02	.3494E+02	.4022E+02	.4586E+02	.5183E+02	.5815E+02	.6480E+02
Z	.7178E+02	.7908E+02	.8669E+02	.9462E+02	.1028E+03	.1114E+03	.1202E+03	.1293E+03	.1386E+03	.1482E+03
Z	.1581E+03	.1683E+03	.1787E+03	.1893E+03	.2001E+03	.2112E+03	.2225E+03	.2340E+03	.2457E+03	.2577E+03
Z	.2699E+03	.2820E+03	.2945E+03	.3072E+03	.3200E+03	.3329E+03	.3461E+03	.3593E+03	.3728E+03	.3863E+03
Z	.4000E+03	.4138E+03	.4278E+03	.4419E+03	.4560E+03	.4703E+03	.4847E+03	.4992E+03	.5138E+03	.5285E+03
Z	.5433E+03	.5582E+03	.5731E+03	.5881E+03	.6033E+03	.6184E+03	.6337E+03	.6490E+03	.6644E+03	.6798E+03
Z	.6953E+03	.7109E+03	.7265E+03	.7422E+03	.7579E+03					
VF	.1000E-07	.1958E+02	.3910E+02	.5855E+02	.7790E+02	.9714E+02	.1163E+03	.1353E+03	.1542E+03	.1729E+03
VF	.1915E+03	.2100E+03	.2283E+03	.2463E+03	.2641E+03	.2816E+03	.2989E+03	.3159E+03	.3325E+03	.3489E+03
VF	.3650E+03	.3807E+03	.3961E+03	.4112E+03	.4259E+03	.4403E+03	.4544E+03	.4680E+03	.4814E+03	.4944E+03
VF	.5070E+03	.5193E+03	.5312E+03	.5428E+03	.5541E+03	.5650E+03	.5755E+03	.5858E+03	.5957E+03	.6052E+03
VF	.6145E+03	.6235E+03	.6321E+03	.6405E+03	.6485E+03	.6563E+03	.6638E+03	.6710E+03	.6780E+03	.6847E+03
VF	.6911E+03	.6974E+03	.7033E+03	.7091E+03	.7146E+03	.7199E+03	.7250E+03	.7299E+03	.7346E+03	.7391E+03
VF	.7435E+03	.7476E+03	.7516E+03	.7554E+03	.7591E+03	.7626E+03	.7660E+03	.7692E+03	.7723E+03	.7753E+03
VF	.7781E+03	.7808E+03	.7834E+03	.7859E+03	.7883E+03					

I= 4 DI= .4986E+00

TF	0.	.2000E-01	.4000E-01	.6000E-01	.8000E-01	.1000E+00	.1200E+00	.1400E+00	.1600E+00	.1800E+00
TF	.2000E+00	.2200E+00	.2400E+00	.2600E+00	.2800E+00	.3000E+00	.3200E+00	.3400E+00	.3600E+00	.3800E+00
TF	.4000E+00	.4200E+00	.4400E+00	.4600E+00	.4800E+00	.5000E+00	.5200E+00	.5400E+00	.5600E+00	.5800E+00
TF	.6000E+00	.6200E+00	.6400E+00	.6600E+00	.6800E+00	.7000E+00	.7200E+00	.7400E+00	.7600E+00	.7800E+00
TF	.8000E+00	.8200E+00	.8400E+00	.8600E+00	.8800E+00	.9000E+00	.9200E+00	.9400E+00	.9600E+00	.9800E+00
TF	.1000E+01	.1020E+01	.1040E+01	.1060E+01	.1080E+01	.1100E+01	.1120E+01	.1140E+01	.1160E+01	.1180E+01
TF	.1200E+01	.1220E+01	.1240E+01	.1260E+01	.1280E+01	.1300E+01	.1320E+01	.1340E+01	.1360E+01	.1380E+01
TF	.1400E+01	.1420E+01								
Z	0.	.2000E-09	.3918E+00	.1175E+01	.2348E+01	.3910E+01	.5860E+01	.8196E+01	.1092E+02	.1402E+02
Z	.1751E+02	.2137E+02	.2561E+02	.3022E+02	.3521E+02	.4055E+02	.4626E+02	.5233E+02	.5874E+02	.6551E+02
Z	.7262E+02	.8007E+02	.8786E+02	.9597E+02	.1044E+03	.1132E+03	.1222E+03	.1316E+03	.1413E+03	.1512E+03
Z	.1615E+03	.1720E+03	.1829E+03	.1940E+03	.2053E+03	.2169E+03	.2288E+03	.2409E+03	.2533E+03	.2659E+03
Z	.2787E+03	.2918E+03	.3051E+03	.3186E+03	.3322E+03	.3461E+03	.3602E+03	.3745E+03	.3890E+03	.4036E+03
Z	.4185E+03	.4334E+03	.4486E+03	.4639E+03	.4794E+03	.4950E+03	.5108E+03	.5267E+03	.5427E+03	.5589E+03
Z	.5752E+03	.5917E+03	.6082E+03	.6249E+03	.6417E+03	.6585E+03	.6755E+03	.6926E+03	.7098E+03	.7271E+03
Z	.7445E+03	.7620E+03								
VF	.1000E-07	.1959E+02	.3914E+02	.5865E+02	.7810E+02	.9749E+02	.1168E+03	.1361E+03	.1552E+03	.1743E+03
VF	.1932E+03	.2120E+03	.2306E+03	.2491E+03	.2673E+03	.2854E+03	.3033E+03	.3209E+03	.3383E+03	.3555E+03
VF	.3725E+03	.3892E+03	.4056E+03	.4218E+03	.4377E+03	.4533E+03	.4687E+03	.4838E+03	.4985E+03	.5130E+03
VF	.5272E+03	.5411E+03	.5547E+03	.5680E+03	.5810E+03	.5937E+03	.6061E+03	.6182E+03	.6300E+03	.6415E+03
VF	.6528E+03	.6637E+03	.6743E+03	.6847E+03	.6948E+03	.7046E+03	.7141E+03	.7234E+03	.7324E+03	.7412E+03
VF	.7496E+03	.7579E+03	.7659E+03	.7736E+03	.7811E+03	.7884E+03	.7955E+03	.8023E+03	.8089E+03	.8154E+03
VF	.8217E+03	.8276E+03	.8334E+03	.8390E+03	.8444E+03	.8497E+03	.8548E+03	.8597E+03	.8644E+03	.8690E+03
VF	.8734E+03	.8777E+03								

I= 5 DI= .6381E+00

TF	0.	.2000E-01	.4000E-01	.6000E-01	.8000E-01	.1000E+00	.1200E+00	.1400E+00	.1600E+00	.1800E+00
TF	.2000E+00	.2200E+00	.2400E+00	.2600E+00	.2800E+00	.3000E+00	.3200E+00	.3400E+00	.3600E+00	.3800E+00
TF	.4000E+00	.4200E+00	.4400E+00	.4600E+00	.4800E+00	.5000E+00	.5200E+00	.5400E+00	.5600E+00	.5800E+00
TF	.6000E+00	.6200E+00	.6400E+00	.6600E+00	.6800E+00	.7000E+00	.7200E+00	.7400E+00	.7600E+00	.7800E+00
TF	.8000E+00	.8200E+00	.8400E+00	.8600E+00	.8800E+00	.9000E+00	.9200E+00	.9400E+00	.9600E+00	.9800E+00
TF	.1000E+01	.1020E+01	.1040E+01	.1060E+01	.1080E+01	.1100E+01	.1120E+01	.1140E+01	.1160E+01	.1180E+01
TF	.1200E+01	.1220E+01	.1240E+01	.1260E+01	.1280E+01	.1300E+01	.1320E+01	.1340E+01	.1360E+01	.1380E+01

```
Z    0.          .1960E+00   .5880E+00   .1371E+01   .2546E+01   .4110E+01   .6063E+01   .8405E+01   .1113E+02   .1425E+02
Z    .1774E+02   .2162E+02   .2588E+02   .3051E+02   .3552E+02   .4090E+02   .4665E+02   .5276E+02   .5923E+02   .6606E+02
Z    .7325E+02   .8078E+02   .8866E+02   .9688E+02   .1054E+03   .1143E+03   .1235E+03   .1331E+03   .1429E+03   .1531E+03
Z    .1636E+03   .1744E+03   .1855E+03   .1968E+03   .2085E+03   .2205E+03   .2327E+03   .2452E+03   .2580E+03   .2710E+03
Z    .2843E+03   .2978E+03   .3116E+03   .3256E+03   .3399E+03   .3544E+03   .3691E+03   .3840E+03   .3992E+03   .4145E+03
Z    .4301E+03   .4459E+03   .4618E+03   .4780E+03   .4943E+03   .5108E+03   .5275E+03   .5444E+03   .5614E+03   .5786E+03
Z    .5960E+03   .6135E+03   .6312E+03   .6490E+03   .6669E+03   .6850E+03   .7033E+03   .7216E+03   .7401E+03   .7587E+03

VF   .1000E-07   .1960E+02   .3917E+02   .5871E+02   .7821E+02   .9767E+02   .1171E+03   .1364E+03   .1557E+03   .1749E+03
VF   .1939E+03   .2129E+03   .2317E+03   .2504E+03   .2690E+03   .2873E+03   .3056E+03   .3236E+03   .3415E+03   .3592E+03
VF   .3767E+03   .3939E+03   .4110E+03   .4279E+03   .4445E+03   .4609E+03   .4771E+03   .4930E+03   .5087E+03   .5241E+03
VF   .5393E+03   .5542E+03   .5689E+03   .5833E+03   .5975E+03   .6113E+03   .6250E+03   .6383E+03   .6514E+03   .6643E+03
VF   .6769E+03   .6892E+03   .7012E+03   .7130E+03   .7245E+03   .7358E+03   .7468E+03   .7576E+03   .7681E+03   .7784E+03
VF   .7884E+03   .7981E+03   .8077E+03   .8170E+03   .8260E+03   .8349E+03   .8435E+03   .8518E+03   .8600E+03   .8679E+03
VF   .8757E+03   .8832E+03   .8905E+03   .8976E+03   .9045E+03   .9112E+03   .9178E+03   .9241E+03   .9303E+03   .9363E+03

I=  6    DI= .7777E+00

TF   0.          .2000E-01   .4000E-01   .6000E-01   .8000E-01   .1000E+00   .1200E+00   .1400E+00   .1600E+00   .1800E+00
TF   .2000E+00   .2200E+00   .2400E+00   .2600E+00   .2800E+00   .3000E+00   .3200E+00   .3400E+00   .3600E+00   .3800E+00
TF   .4000E+00   .4200E+00   .4400E+00   .4600E+00   .4800E+00   .5000E+00   .5200E+00   .5400E+00   .5600E+00   .5800E+00
TF   .6000E+00   .6200E+00   .6400E+00   .6600E+00   .6800E+00   .7000E+00   .7200E+00   .7400E+00   .7600E+00   .7800E+00
TF   .8000E+00   .8200E+00   .8400E+00   .8600E+00   .8800E+00   .9000E+00   .9200E+00   .9400E+00   .9600E+00   .9800E+00
TF   .1000E+01   .1020E+01   .1040E+01   .1060E+01   .1080E+01   .1100E+01   .1120E+01   .1140E+01   .1160E+01   .1180E+01
TF   .1200E+01   .1220E+01   .1240E+01   .1260E+01   .1280E+01   .1300E+01   .1320E+01   .1340E+01   .1360E+01

Z    0.          .1960E+00   .5880E+00   .1372E+01   .2546E+01   .4111E+01   .6066E+01   .8411E+01   .1114E+02   .1426E+02
Z    .1776E+02   .2165E+02   .2592E+02   .3057E+02   .3559E+02   .4099E+02   .4676E+02   .5290E+02   .5941E+02   .6628E+02
Z    .7351E+02   .8109E+02   .8903E+02   .9732E+02   .1060E+03   .1149E+03   .1243E+03   .1339E+03   .1439E+03   .1542E+03
Z    .1648E+03   .1758E+03   .1870E+03   .1986E+03   .2105E+03   .2226E+03   .2351E+03   .2479E+03   .2609E+03   .2742E+03
Z    .2878E+03   .3017E+03   .3158E+03   .3302E+03   .3449E+03   .3598E+03   .3749E+03   .3903E+03   .4060E+03   .4218E+03
Z    .4379E+03   .4543E+03   .4708E+03   .4875E+03   .5045E+03   .5217E+03   .5390E+03   .5566E+03   .5744E+03   .5923E+03
Z    .6104E+03   .6287E+03   .6472E+03   .6659E+03   .6847E+03   .7037E+03   .7229E+03   .7421E+03   .7616E+03

VF   .1000E-07   .1960E+02   .3918E+02   .5873E+02   .7826E+02   .9776E+02   .1172E+03   .1366E+03   .1559E+03   .1752E+03
VF   .1943E+03   .2134E+03   .2324E+03   .2512E+03   .2699E+03   .2885E+03   .3070E+03   .3253E+03   .3435E+03   .3615E+03
VF   .3793E+03   .3970E+03   .4145E+03   .4318E+03   .4489E+03   .4658E+03   .4826E+03   .4991E+03   .5154E+03   .5315E+03
VF   .5473E+03   .5630E+03   .5784E+03   .5936E+03   .6086E+03   .6233E+03   .6378E+03   .6521E+03   .6661E+03   .6799E+03
VF   .6935E+03   .7068E+03   .7199E+03   .7327E+03   .7453E+03   .7577E+03   .7698E+03   .7817E+03   .7933E+03   .8048E+03
VF   .8159E+03   .8269E+03   .8376E+03   .8481E+03   .8584E+03   .8684E+03   .8782E+03   .8879E+03   .8972E+03   .9064E+03
VF   .9154E+03   .9241E+03   .9327E+03   .9411E+03   .9492E+03   .9572E+03   .9649E+03   .9725E+03   .9799E+03

I=  7    DI= .9174E+00

TF   0.          .2000E-01   .4000E-01   .6000E-01   .8000E-01   .1000E+00   .1200E+00   .1400E+00   .1600E+00   .1800E+00
TF   .2000E+00   .2200E+00   .2400E+00   .2600E+00   .2800E+00   .3000E+00   .3200E+00   .3400E+00   .3600E+00   .3800E+00
TF   .4000E+00   .4200E+00   .4400E+00   .4600E+00   .4800E+00   .5000E+00   .5200E+00   .5400E+00   .5600E+00   .5800E+00
TF   .6000E+00   .6200E+00   .6400E+00   .6600E+00   .6800E+00   .7000E+00   .7200E+00   .7400E+00   .7600E+00   .7800E+00
TF   .8000E+00   .8200E+00   .8400E+00   .8600E+00   .8800E+00   .9000E+00   .9200E+00   .9400E+00   .9600E+00   .9800E+00
TF   .1000E+01   .1020E+01   .1040E+01   .1060E+01   .1080E+01   .1100E+01   .1120E+01   .1140E+01   .1160E+01   .1180E+01
TF   .1200E+01   .1220E+01   .1240E+01   .1260E+01   .1280E+01   .1300E+01   .1320E+01   .1340E+01

Z    0.          .1960E+00   .5880E+00   .1372E+01   .2547E+01   .4112E+01   .6069E+01   .8414E+01   .1115E+02   .1427E+02
Z    .1778E+02   .2167E+02   .2594E+02   .3060E+02   .3564E+02   .4105E+02   .4684E+02   .5300E+02   .5953E+02   .6642E+02
Z    .7369E+02   .8131E+02   .8929E+02   .9763E+02   .1063E+03   .1154E+03   .1248E+03   .1345E+03   .1445E+03   .1550E+03
```

```
     Z     .1657E+03  .1747E+03  .1881E+03  .1998E+03  .2119E+03  .2242E+03  .2368E+03  .2498E+03  .2630E+03  .2766E+03
     Z     .2904E+03  .3045E+03  .3189E+03  .3336E+03  .3485E+03  .3637E+03  .3792E+03  .3949E+03  .4109E+03  .4272E+03
     Z     .4436E+03  .4604E+03  .4773E+03  .4945E+03  .5120E+03  .5296E+03  .5475E+03  .5656E+03  .5839E+03  .6024E+03
     Z     .6211E+03  .6401E+03  .6592E+03  .6785E+03  .6980E+03  .7176E+03  .7375E+03  .7575E+03

     VF    .1000E-07  .1960E+02  .3918E+02  .5875E+02  .7829E+02  .9781E+02  .1173E+03  .1367E+03  .1561E+03  .1754E+03
     VF    .1946E+03  .2137E+03  .2328E+03  .2518E+03  .2706E+03  .2894E+03  .3080E+03  .3265E+03  .3449E+03  .3631E+03
     VF    .3812E+03  .3992E+03  .4170E+03  .4346E+03  .4520E+03  .4693E+03  .4865E+03  .5034E+03  .5202E+03  .5367E+03
     VF    .5531E+03  .5693E+03  .5853E+03  .6010E+03  .6166E+03  .6320E+03  .6471E+03  .6621E+03  .6768E+03  .6913E+03
     VF    .7056E+03  .7197E+03  .7336E+03  .7472E+03  .7606E+03  .7738E+03  .7868E+03  .7996E+03  .8121E+03  .8244E+03
     VF    .8366E+03  .8484E+03  .8601E+03  .8716E+03  .8828E+03  .8938E+03  .9047E+03  .9153E+03  .9256E+03  .9358E+03
     VF    .9458E+03  .9556E+03  .9652E+03  .9746E+03  .9837E+03  .9927E+03  .1002E+04  .1010E+04

I=  8    DI= .1057E+01

     TF    0.         .2000E-01  .4000E-01  .6000E-01  .8000E-01  .1000E+00  .1200E+00  .1400E+00  .1600E+00  .1800E+00
     TF    .2000E+00  .2200E+00  .2400E+00  .2600E+00  .2800E+00  .3000E+00  .3200E+00  .3400E+00  .3600E+00  .3800E+00
     TF    .4000E+00  .4200E+00  .4400E+00  .4600E+00  .4800E+00  .5000E+00  .5200E+00  .5400E+00  .5600E+00  .5800E+00
     TF    .6000E+00  .6200E+00  .6400E+00  .6600E+00  .6800E+00  .7000E+00  .7200E+00  .7400E+00  .7600E+00  .7800E+00
     TF    .8000E+00  .8200E+00  .8400E+00  .8600E+00  .8800E+00  .9000E+00  .9200E+00  .9400E+00  .9600E+00  .9800E+00
     TF    .1000E+01  .1020E+01  .1040E+01  .1060E+01  .1080E+01  .1100E+01  .1120E+01  .1140E+01  .1160E+01  .1180E+01
     TF    .1200E+01  .1220E+01  .1240E+01  .1260E+01  .1280E+01  .1300E+01  .1320E+01

     Z     0.         .1960E+00  .5880E+00  .1372E+01  .2547E+01  .4113E+01  .6070E+01  .8417E+01  .1115E+02  .1428E+02
     Z     .1779E+02  .2168E+02  .2596E+02  .3062E+02  .3567E+02  .4109E+02  .4689E+02  .5306E+02  .5961E+02  .6653E+02
     Z     .7382E+02  .8147E+02  .8948E+02  .9786E+02  .1066E+03  .1157E+03  .1251E+03  .1349E+03  .1450E+03  .1555E+03
     Z     .1663E+03  .1775E+03  .1890E+03  .2008E+03  .2129E+03  .2254E+03  .2381E+03  .2512E+03  .2646E+03  .2783E+03
     Z     .2923E+03  .3066E+03  .3212E+03  .3361E+03  .3512E+03  .3667E+03  .3824E+03  .3984E+03  .4147E+03  .4312E+03
     Z     .4480E+03  .4651E+03  .4824E+03  .4999E+03  .5177E+03  .5357E+03  .5540E+03  .5725E+03  .5913E+03  .6102E+03
     Z     .6294E+03  .6488E+03  .6684E+03  .6882E+03  .7083E+03  .7285E+03  .7489E+03

     VF    .1000E-07  .1960E+02  .3919E+02  .5876E+02  .7831E+02  .9784E+02  .1173E+03  .1368E+03  .1562E+03  .1755E+03
     VF    .1948E+03  .2140E+03  .2331E+03  .2522E+03  .2711E+03  .2900E+03  .3087E+03  .3274E+03  .3459E+03  .3643E+03
     VF    .3826E+03  .4008E+03  .4188E+03  .4367E+03  .4544E+03  .4720E+03  .4894E+03  .5066E+03  .5237E+03  .5407E+03
     VF    .5574E+03  .5740E+03  .5904E+03  .6066E+03  .6227E+03  .6385E+03  .6542E+03  .6696E+03  .6849E+03  .7000E+03
     VF    .7149E+03  .7296E+03  .7440E+03  .7583E+03  .7724E+03  .7863E+03  .7999E+03  .8134E+03  .8267E+03  .8397E+03
     VF    .8526E+03  .8652E+03  .8777E+03  .8899E+03  .9019E+03  .9137E+03  .9254E+03  .9368E+03  .9480E+03  .9591E+03
     VF    .9699E+03  .9805E+03  .9910E+03  .1001E+04  .1011E+04  .1021E+04  .1031E+04

I=  9    DI= .1197E+01

     TF    0.         .2000E-01  .4000E-01  .6000E-01  .8000E-01  .1000E+00  .1200E+00  .1400E+00  .1600E+00  .1800E+00
     TF    .2000E+00  .2200E+00  .2400E+00  .2600E+00  .2800E+00  .3000E+00  .3200E+00  .3400E+00  .3600E+00  .3800E+00
     TF    .4000E+00  .4200E+00  .4400E+00  .4600E+00  .4800E+00  .5000E+00  .5200E+00  .5400E+00  .5600E+00  .5800E+00
     TF    .6000E+00  .6200E+00  .6400E+00  .6600E+00  .6800E+00  .7000E+00  .7200E+00  .7400E+00  .7600E+00  .7800E+00
     TF    .8000E+00  .8200E+00  .8400E+00  .8600E+00  .8800E+00  .9000E+00  .9200E+00  .9400E+00  .9600E+00  .9800E+00
     TF    .1000E+01  .1020E+01  .1040E+01  .1060E+01  .1080E+01  .1100E+01  .1120E+01  .1140E+01  .1160E+01  .1180E+01
     TF    .1200E+01  .1220E+01  .1240E+01  .1260E+01  .1280E+01  .1300E+01  .1320E+01

     Z     0.         .1960E+00  .7840E+00  .1568E+01  .2744E+01  .4310E+01  .6268E+01  .8615E+01  .1135E+02  .1448E+02
     Z     .1799E+02  .2189E+02  .2617E+02  .3084E+02  .3589E+02  .4132E+02  .4713E+02  .5332E+02  .5988E+02  .6681E+02
     Z     .7412E+02  .8179E+02  .8983E+02  .9823E+02  .1070E+03  .1161E+03  .1256E+03  .1354E+03  .1456E+03  .1562E+03
     Z     .1670E+03  .1782E+03  .1898E+03  .2017E+03  .2139E+03  .2265E+03  .2393E+03  .2525E+03  .2660E+03  .2799E+03
     Z     .2940E+03  .3084E+03  .3232E+03  .3382E+03  .3536E+03  .3692E+03  .3851E+03  .4013E+03  .4178E+03  .4346E+03
     Z     .4516E+03  .4689E+03  .4865E+03  .5043E+03  .5224E+03  .5408E+03  .5594E+03  .5782E+03  .5973E+03  .6166E+03
     Z     .6362E+03  .6560E+03  .6760E+03  .6962E+03  .7167E+03  .7374E+03  .7582E+03
```

```
VF     .1000E-07  .1960E+02  .3920E+02  .5878E+02  .7834E+02  .9787E+02  .1174E+03  .1368E+03  .1563E+03  .1756E+03
VF     .1949E+03  .2142E+03  .2334E+03  .2525E+03  .2715E+03  .2905E+03  .3093E+03  .3281E+03  .3467E+03  .3653E+03
VF     .3837E+03  .4020E+03  .4202E+03  .4383E+03  .4562E+03  .4740E+03  .4917E+03  .5092E+03  .5265E+03  .5437E+03
VF     .5608E+03  .5777E+03  .5944E+03  .6110E+03  .6274E+03  .6437E+03  .6597E+03  .6756E+03  .6913E+03  .7069E+03
VF     .7222E+03  .7374E+03  .7523E+03  .7671E+03  .7817E+03  .7962E+03  .8104E+03  .8244E+03  .8383E+03  .8519E+03
VF     .8654E+03  .8786E+03  .8917E+03  .9046E+03  .9173E+03  .9298E+03  .9421E+03  .9542E+03  .9661E+03  .9778E+03
VF     .9894E+03  .1001E+04  .1012E+04  .1023E+04  .1034E+04  .1044E+04  .1055E+04

I= 10    DI= .1336E+01

TF     0.         .2000E-01  .4000E-01  .6000E-01  .8000E-01  .1000E+00  .1200E+00  .1400E+00  .1600E+00  .1800E+00
TF     .2000E+00  .2200E+00  .2400E+00  .2600E+00  .2800E+00  .3000E+00  .3200E+00  .3400E+00  .3600E+00  .3800E+00
TF     .4000E+00  .4200E+00  .4400E+00  .4600E+00  .4800E+00  .5000E+00  .5200E+00  .5400E+00  .5600E+00  .5800E+00
TF     .6000E+00  .6200E+00  .6400E+00  .6600E+00  .6800E+00  .7000E+00  .7200E+00  .7400E+00  .7600E+00  .7800E+00
TF     .8000E+00  .8200E+00  .8400E+00  .8600E+00  .8800E+00  .9000E+00  .9200E+00  .9400E+00  .9600E+00  .9800E+00
TF     .1000E+01  .1020E+01  .1040E+01  .1060E+01  .1080E+01  .1100E+01  .1120E+01  .1140E+01  .1160E+01  .1180E+01
TF     .1200E+01  .1220E+01  .1240E+01  .1260E+01  .1280E+01  .1300E+01

Z      0.         .1960E+00  .7840E+00  .1568E+01  .2744E+01  .4311E+01  .6268E+01  .8616E+01  .1135E+02  .1448E+02
Z      .1799E+02  .2190E+02  .2618E+02  .3085E+02  .3591E+02  .4134E+02  .4716E+02  .5336E+02  .5993E+02  .6687E+02
Z      .7419E+02  .8189E+02  .8995E+02  .9837E+02  .1072E+03  .1163E+03  .1258E+03  .1357E+03  .1459E+03  .1565E+03
Z      .1674E+03  .1787E+03  .1903E+03  .2023E+03  .2145E+03  .2272E+03  .2401E+03  .2534E+03  .2670E+03  .2809E+03
Z      .2952E+03  .3098E+03  .3246E+03  .3398E+03  .3553E+03  .3711E+03  .3872E+03  .4035E+03  .4202E+03  .4372E+03
Z      .4544E+03  .4719E+03  .4897E+03  .5078E+03  .5261E+03  .5447E+03  .5636E+03  .5827E+03  .6021E+03  .6217E+03
Z      .6415E+03  .6617E+03  .6820E+03  .7026E+03  .7234E+03  .7445E+03

VF     .1000E-07  .1960E+02  .3920E+02  .5878E+02  .7835E+02  .9789E+02  .1174E+03  .1369E+03  .1563E+03  .1757E+03
VF     .1951E+03  .2143E+03  .2336E+03  .2527E+03  .2718E+03  .2908E+03  .3098E+03  .3286E+03  .3473E+03  .3660E+03
VF     .3845E+03  .4030E+03  .4213E+03  .4395E+03  .4576E+03  .4756E+03  .4935E+03  .5112E+03  .5288E+03  .5462E+03
VF     .5635E+03  .5807E+03  .5977E+03  .6145E+03  .6312E+03  .6478E+03  .6642E+03  .6804E+03  .6965E+03  .7124E+03
VF     .7281E+03  .7437E+03  .7591E+03  .7743E+03  .7893E+03  .8042E+03  .8189E+03  .8334E+03  .8477E+03  .8619E+03
VF     .8758E+03  .8896E+03  .9032E+03  .9166E+03  .9299E+03  .9429E+03  .9558E+03  .9685E+03  .9810E+03  .9934E+03
VF     .1006E+04  .1017E+04  .1029E+04  .1041E+04  .1052E+04  .1064E+04

I= 11    DI= .1476E+01

TF     0.         .2000E-01  .4000E-01  .6000E-01  .8000E-01  .1000E+00  .1200E+00  .1400E+00  .1600E+00  .1800E+00
TF     .2000E+00  .2200E+00  .2400E+00  .2600E+00  .2800E+00  .3000E+00  .3200E+00  .3400E+00  .3600E+00  .3800E+00
TF     .4000E+00  .4200E+00  .4400E+00  .4600E+00  .4800E+00  .5000E+00  .5200E+00  .5400E+00  .5600E+00  .5800E+00
TF     .6000E+00  .6200E+00  .6400E+00  .6600E+00  .6800E+00  .7000E+00  .7200E+00  .7400E+00  .7600E+00  .7800E+00
TF     .8000E+00  .8200E+00  .8400E+00  .8600E+00  .8800E+00  .9000E+00  .9200E+00  .9400E+00  .9600E+00  .9800E+00
TF     .1000E+01  .1020E+01  .1040E+01  .1060E+01  .1080E+01  .1100E+01  .1120E+01  .1140E+01  .1160E+01  .1180E+01
TF     .1200E+01  .1220E+01  .1240E+01  .1260E+01  .1280E+01  .1300E+01

Z      0.         .1960E+00  .7840E+00  .1568E+01  .2744E+01  .4311E+01  .6269E+01  .8617E+01  .1136E+02  .1448E+02
Z      .1800E+02  .2190E+02  .2619E+02  .3086E+02  .3592E+02  .4136E+02  .4719E+02  .5339E+02  .5997E+02  .6693E+02
Z      .7426E+02  .8196E+02  .9004E+02  .9848E+02  .1073E+03  .1165E+03  .1260E+03  .1359E+03  .1462E+03  .1568E+03
Z      .1677E+03  .1791E+03  .1907E+03  .2027E+03  .2151E+03  .2278E+03  .2408E+03  .2541E+03  .2678E+03  .2818E+03
Z      .2962E+03  .3108E+03  .3258E+03  .3411E+03  .3567E+03  .3726E+03  .3888E+03  .4054E+03  .4222E+03  .4393E+03
Z      .4567E+03  .4744E+03  .4924E+03  .5106E+03  .5291E+03  .5480E+03  .5670E+03  .5864E+03  .6060E+03  .6259E+03
Z      .6460E+03  .6664E+03  .6870E+03  .7079E+03  .7290E+03  .7504E+03

VF     .1000E-07  .1960E+02  .3920E+02  .5878E+02  .7835E+02  .9790E+02  .1174E+03  .1369E+03  .1564E+03  .1758E+03
VF     .1951E+03  .2145E+03  .2337E+03  .2529E+03  .2721E+03  .2911E+03  .3101E+03  .3290E+03  .3478E+03  .3666E+03
VF     .3852E+03  .4038E+03  .4222E+03  .4406E+03  .4588E+03  .4769E+03  .4949E+03  .5128E+03  .5306E+03  .5482E+03
VF     .5657E+03  .5831E+03  .6003E+03  .6174E+03  .6344E+03  .6512E+03  .6679E+03  .6844E+03  .7007E+03  .7169E+03
VF     .7330E+03  .7489E+03  .7646E+03  .7802E+03  .7956E+03  .8108E+03  .8259E+03  .8408E+03  .8556E+03  .8701E+03
```

VF .8845E+03 .8988E+03 .9128E+03 .9267E+03 .9404E+03 .9540E+03 .9673E+03 .9805E+03 .9936E+03 .1006E+04
VF .1019E+04 .1032E+04 .1044E+04 .1056E+04 .1068E+04 .1080E+04

HD .1622E-01 .5873E+00 .1570E+01 .1847E+01 .1443E+01 .8823E+00 .4578E+00 .2113E+00 .8931E-01 .3524E-01
HD .1317E-01

TIME= .50000E+01 SECONDS

P= .43158E-01 TG= .35911E+02 TW= .23903E+02 YOC= .78841E-02 BRS= .17475E+00 SBR= .29412E+02

Q= .38408E+03 SQ= .16331E+06 QW= .60688E+03 SQW= .16326E+04 MOLO= .21570E+02 MOLG= .27358E+04

SML= .34003E+04

TIME= .10000E+02 SECONDS

P= .42405E-01 TG= .35703E+02 TW= .23908E+02 YOC= .78837E-02 BRS=0. SBR= .29502E+02

Q=0. SQ= .16351E+06 QW= .59609E+03 SQW= .46415E+04 MOLO= .21569E+02 MOLG= .27358E+04

SML= .34003E+04

TIME= .15000E+02 SECONDS

P= .41616E-01 TG= .35484E+02 TW= .23914E+02 YOC= .78837E-02 BRS=0. SBR= .29502E+02

Q=0. SQ= .16351E+06 QW= .58474E+03 SQW= .75933E+04 MOLO= .21569E+02 MOLG= .27358E+04

SML= .34003E+04

TIME= .20000E+02 SECONDS

P= .40842E-01 TG= .35269E+02 TW= .23919E+02 YOC= .78837E-02 BRS=0. SBR= .29502E+02

Q=0. SQ= .16351E+06 QW= .57361E+03 SQW= .10489E+05 MOLO= .21569E+02 MOLG= .27358E+04

SML= .34003E+04

TIME= .25000E+02 SECONDS

P= .40082E-01 TG= .35058E+02 TW= .23924E+02 YOC= .78837E-02 BRS=0. SBR= .29502E+02

Q=0. SQ= .16351E+06 QW= .56270E+03 SQW= .13330E+05 MOLO= .21569E+02 MOLG= .27358E+04

SML= .34003E+04

TIME= .30000E+02 SECONDS

P= .39337E-01 TG= .34851E+02 TW= .23929E+02 YOC= .78837E-02 BRS=0. SBR= .29502E+02

Q=0. SQ= .16351E+06 QW= .55199E+03 SQW= .16116E+05 MOLO= .21569E+02 MOLG= .27358E+04

SML= .34003E+04

TIME= .35000E+02 SECONDS

P= .38605E-01 TG= .34648E+02 TW= .23934E+02 YOC= .78837E-02 BRS=0. SBR= .29502E+02

Q=0. SQ= .16351E+06 QW= .54148E+03 SQW= .18850E+05 MOLO= .21569E+02 MOLG= .27358E+04

SML= .34003E+04

TIME= .40000E+02 SECONDS

P= .37888E-01 TG= .34449E+02 TW= .23939E+02 YOC= .78837E-02 BRS=0. SBR= .29502E+02

Q=0. SQ= .16351E+06 QW= .53117E+03 SQW= .21531E+05 MOLO= .21569E+02 MOLG= .27358E+04

SML= .34003E+04

TIME= .45000E+02 SECONDS

P= .37184E-01 TG= .34254E+02 TW= .23944E+02 YOC= .78837E-02 BRS=0. SBR= .29502E+02

Q=0. SQ= .16351E+06 QW= .52106E+03 SQW= .24161E+05 MOLO= .21569E+02 MOLG= .27358E+04

SML= .34003E+04

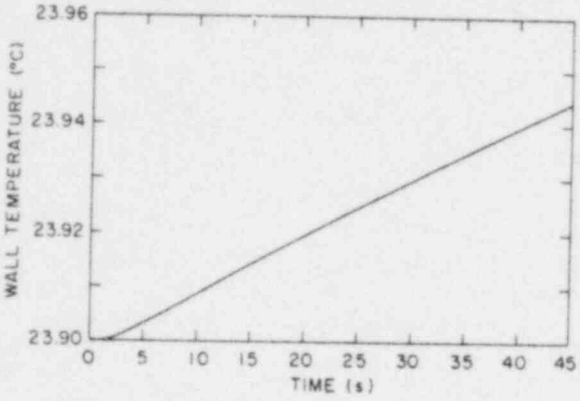

Figure 30. Sample Problem Output - NACOM Prediction of Wall Temperature History for LTV Jet Test No. 8

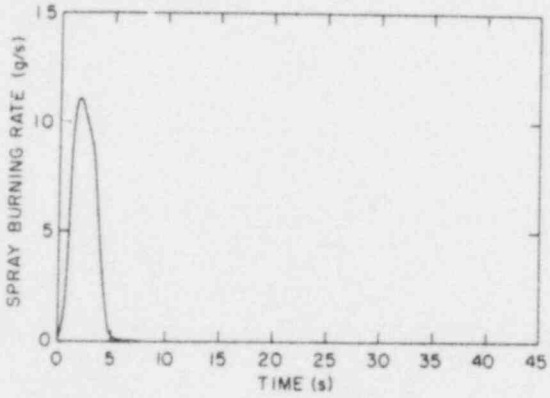

Figure 31. Sample Problem Output - NACOM Prediction of Spray Burning Rate for LTV Jet Test No. 8

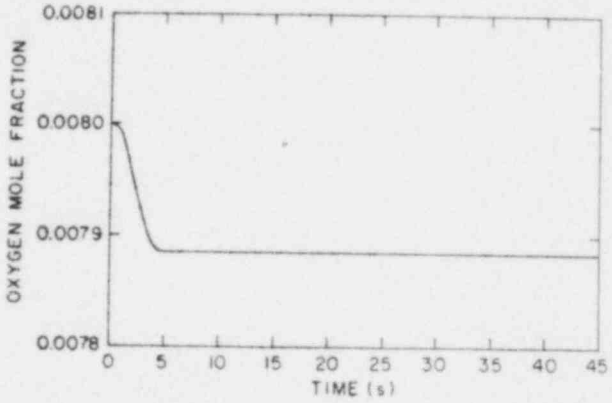

Figure 32. Sample Problem Output - NACOM Prediction of Oxygen Mole Fraction for LTV Jet Test No. 8

APPENDIX D

NACOM CODE LISTING

```
      PROGRAM NACOM(INPUT,OUTPUT)
C
C  NACOM IS A COMPUTER PROGRAM WHICH SIMULATES SODIUM SPRAY FIRES
C  IN LMFBR CONTAINMENT CELLS AS A RESULT OF POSTULATED PIPE RUPTURES.
C
      DIMENSION TITLE(7),DL(2)
      COMMON /NMRH/DT,MOLO,MOLG,R,TG,VOL,YOC
      COMMON /NMR/D(11),ENA,HI,IDU,II(11)
      COMMON /NRH/AI,HRS,P,Q
      COMMON /NR/A,AML(40),R,DD(11,600),DM(11,600),DN(11,600),HC,
     1HFG,IP,IQ,N,NPRT,RD(11),SML,T,TB,TEND,TL(40),TS(11,600),TSI
      COMMON /NM/DME,H,PI,RHOL
      COMMON /NR/ALI,CPS,QW,TW
      REAL NA2O2
      REAL MOLO,MOLG
      DATA R/82.054/,HFG/1005./
      READ 36,IQ,TITLE
C
C  READ INPUT DATA.
C
      READ 37,ALI,H,VOL,DME,ENA,TSI
      READ 37,PI,TGI,YOI,TMAX,TEND,X
      READ 38,NA2O2,CPS,NPRT,IP
C
      IF(IP.EQ.0) GO TO 47
      DO 46 I=1,IP
   46 READ 40,TL(I),AML(I)
   47 PRINT 41,TITLE
      PRINT 42
      PRINT 43,ALI,H,VOL,DME,ENA,TSI,PI,TGI,YOI,TMAX,TEND,X,
     1NA2O2,CPS,NPRT,IP
      IF(IP.EQ.0) GO TO 55
      PRINT 51
      DO 52 I=1,IP
   52 PRINT 53,TL(I),AML(I)
   55 DT=0.01*X
      ALI=ALI*10000.
      H=H*100.
      VOL=VOL*1000000.
      TG=TGI+273.
      TB=1154.
      P=PI
      YOC=YOI
      TW=TG
      T=0.
      N=0
      SBR=0.
      SQ=0.
      SQW=0.
      SML=0.
      S=1.347R*NA2O2/(1.6957-0.3479*NA2O2)
      HC=(1.-S)*2194.5+S*2500.
      AI=S/1.4375+(1.-S)/2.875
      RHOL=0.949-2.23E-4*TSI-1.75E-8*TSI**2
      A=3.14159/6.*RHOL
      IM=TMAX/DT
C
C  SELECTION OF DROP SIZES.
C
      DO 200 L=1,2
      IF(L.EQ.1) DL(1)=DME*4.
      IF(L.EQ.2) DL(2)=DME/4.
      DO 201 M=1,20
```

```
      AB=EXP(3.915*(1.-DL(L)/DME))
      F=(DL(L)/DME)**5*AB-0.01
      IF(F.LT.1.E-6) GO TO 200
      FP=(5.*DL(L)**4/DME**5-(DL(L)/DME)**5*3.915/DME)*AB
  201 DL(L)=DL(L)-F/FP
  200 CONTINUE
      ID=10
      IDD=ID+1
      HI=(DL(1)-DL(2))/ID
      DO 120 I=1,IDD
  120 D(I)=(I-1)*HI+DL(2)
C
      CALL MOTION
      DO 110 I=1,IDD
      JJ=II(I)
C
C  COMPUTE DROP SIZE DISTRIBUTION.
C
      RD(I)=(3.915/DME)**6*D(I)**5/120.*EXP(-3.915*D(I)/DME)
C
      DO 110 J=1,JJ
      TS(I,J)=0.
      DN(I,J)=0.
      DM(I,J)=0.
  110 DD(I,J)=0.
      PRINT 130
      PRINT 100,(RD(I),I=1,IDD)
      DO 45 I=1,IM
      T=T+DT
      N=N+1
      IF(N.LT.NPRT) GO TO 300
      PRINT 80,T
  300 CALL RATES
      CALL BALANCE
      SBR=SBR+BRS*DT
      SQ=SQ+Q*DT
      SQW=SQW+QW*DT
      PP=P-PI
      TGG=TG-273.
      TWW=TW-273.
      IF(N.LT.NPRT) GO TO 45
      PRINT 90,PP,TGG,TWW,YOC,BRS,SBR,Q,SQ,QW,SQW,MOLO,MOLG,SML
      N=0
   45 CONTINUE
   36 FORMAT(I1,7A10)
   37 FORMAT(6F12.4)
   38 FORMAT(2F12.4,2I12)
   40 FORMAT(2F12.4)
   41 FORMAT(1H1,10X,7A10///)
   42 FORMAT(50X,"INPUT LISTING"/)
   43 FORMAT(10X,"ALI=",E10.4,3X,"H=",E10.4,3X,"VOL=",E10.4,
     13X,"DME=",E10.4,3X,"FNA=",E10.4,3X,"TSI=",E10.4//
     210X,"PI=",E10.4,3X,"TGI=",E10.4,3X,"YOI=",E10.4,
     33X,"TMAX=",E10.4,3X,"TEND=",E10.4,3X,"X=",E10.4//
     410X,"NA2O2=",E10.4,3X,"CPS=",E10.4,3X,"NPRT=",
     5I5,3X,"IP=",I5////)
   51 FORMAT(15X,"TIME(S)        FLOW RATE(G/S)")
   53 FORMAT(11X,E12.4,6X,E12.4)
   80 FORMAT(///44X,"TIME=",E11.5,1X,"SECONDS"/)
   90 FORMAT(10X,"P=",E11.5,3X,"TG=",E11.5,3X,"TW=",E11.5,3X,
     1"YOC=",E11.5,3X,"BRS=",E11.5,4X,"SBR=",E11.5//10X,"Q=",E11.5,
     23X,"SQ=",E11.5,3X,"QW=",E11.5,3X,"SQW=",E11.5,3X,"MOLO=",E11.5
     3,3X,"MOLG=",E11.5//10X,"SML=",E11.5///)
```

```
  100 FORMAT(10X,"RD",2X,10E10.4)
  130 FORMAT(//)
      STOP
      END
      SUBROUTINE MOTION
C
C   THIS SUBROUTINE COMPUTES THE DROPLET VELOCITIES BY INTEGRATING
C   THE EQUATION OF MOTION FOR THE DROPLETS.
C
      DIMENSION TF(11,600),Z(11,600)
      COMMON /NMRB/DT,MOLO,MOLG,R,TG,VOL,YOC
      COMMON /NMR/D(11),FNA,HI,IDD,II(11)
      COMMON /MRB/RHOG,GM,VF(11,600)
      COMMON /NM/DME,H,PI,RHOL
      REAL MOLO,MOLG,MUG
      MOLG=PI*VOL/(R*TG)
      MOLG=MOLG*YOC
      GM=(MOLG-MOLO)*28.016+MOLO*32.
      RHOG=GM/VOL
      MUG=6.2E-6*TG**0.66
      DO 40 I=1,IDD
      RP=3.*RHOG/(4.*RHOL*D(I))
      DRM=D(I)*RHOG/MUG
      VF(I,1)=1.E-8
      TF(I,1)=0.
      Z(I,1)=0.
      NN=0
C
C   RUNGE-KUTTA METHOD TO SOLVE THE EQUATION OF MOTION FOR DROPLET VELOCITY.
C
      DO 10 J=1,599
      TF(I,J+1)=TF(I,J)+DT
      IF(NN.EQ.1) GO TO 200
      VF(I,J+1)=980.*TF(I,J+1)
      Z(I,J+1)=490.*TF(I,J+1)**2
      REV=VF(I,J+1)*DRM
      DRAG=RP*VF(I,J+1)**2*CD(REV)
      IF(DRAG.LT.1.) GO TO 110
      NN=1
  200 X=VF(I,J)
      REV=X*DRM
      DRAG=RP*X**2*CD(REV)
      P1=(980.-DRAG)*DT
      X=VF(I,J)+P1/2.
      REV=X*DRM
      P2=(980.-RP*X**2*CD(REV))*DT
      X=VF(I,J)+P2/2.
      REV=X*DRM
      P3=(980.-RP*X**2*CD(REV))*DT
      X=VF(I,J)+P3
      REV=X*DRM
      P4=(980.-RP*X**2*CD(REV))*DT
      VF(I,J+1)=VF(I,J)+(P1+2.*P2+2.*P3+P4)/6.
      Z(I,J+1)=Z(I,J)+VF(I,J)*DT
  110 IF(Z(I,J+1).GE.H) GO TO 70
   10 CONTINUE
   70 II(I)=J
      PRINT 25,I,D(I)
      PRINT 30,(TF(I,K),K=1,J)
      PRINT 80
      PRINT 45,(Z(I,K),K=1,J)
      PRINT 80
      PRINT 60,(VF(I,K),K=1,J)
```

```
   40 CONTINUE
   25 FORMAT(//5X,"I=",I3,4X,"DI=",E10.4/)
   30 FORMAT(10X,"TF",2X,10E11.4)
   45 FORMAT(10X,"Z",3X,10E11.4)
   60 FORMAT(10X,"VF",2X,10E11.4)
   80 FORMAT(/)
      RETURN
      END
      FUNCTION CD(REV)
C
C  STANDARD DRAG COEFFICIENT CORRELATIONS.
C
C
      IF(REV.LT.0.1) CD=24./REV
      IF(REV.GE.0.1.AND.REV.LT.6.) CD=7.6+23.71/REV
      IF(REV.GE.6..AND.REV.LT.500.) CD=18.5/REV**0.6
      IF(REV.GE.500.) CD=4./9.
      RETURN
      END
      SUBROUTINE RATES
C
C  THIS IS TO CALCULATE THE BURNING RATE OF SODIUM SPRAY AND TOTAL HEAT
C  RELEASED BY SPRAY COMBUTION.
C
      DIMENSION RE(600),QC(600),QG(600),TSS(600)
      DIMENSION BRF(600),QIN(600)
      COMMON /NMRR/DT,MOLO,MOLG,R,TG,VOL,YOC
      COMMON /NMR/D(11),FNA,HI,IDD,II(11)
      COMMON /NRB/AI,BRS,P,Q
      COMMON /NR/A,AML(40),H,DD(11,600),DM(11,600),DN(11,600),HC,
     1HFG,IP,IQ,N,NPRT,RD(11),SML,T,TB,TEND,TL(40),TS(11,600),TSI
      COMMON /MRB/RHOG,GM,VF(11,600)
      REAL MOLO,MOLG,MUG
      MOLG=P*VOL/(R*TG)
      MOLO=MOLG*YOC
      GM=(MOLG-MOLO)*28.016+MOLO*32.
      YO=MOLO*32./GM
      RHOG=GM/VOL
      TA=(TG+TH)/2.
      CPG=0.2315+4.61E-5*TA
      AKG=1.05E-6*TA**0.71852
      MUG=4.2E-6*TA**0.66
      PR=CPG*MUG/AKG
      A2=PR**0.3333
      DP=1.849E-5*TA**1.645/P
      CDP=2.25E-7*TA**0.645
      SC=MUG/(RHOG*DP)
      R=HC*YO/HFG/AI+CPG*(TG-TB)/HFG
      Q=0.
      BRS=0.
C
C  COMPUTE THE SODIUM LEAK RATE.
C
      IF(T.GE.TEND) GO TO 101
      IF(IP.EQ.0) GO TO 100
      DO 30 K=1,IP
      IF((TL(K)-T).GT.0.) GO TO 40
   30 CONTINUE
      AM=AML(IP)
      GO TO 70
   40 AM=(AML(K)-AML(K-1))/(TL(K)-TL(K-1))*(T-TL(K-1))+AML(K-1)
      GO TO 70
  100 AM=FNA
```

```
      GO TO 70
  101 AM=0.
   70 SML=SML+AM*DT
C
      DO 10 I=1,IDD
      JJ=II(I)
      DMI=A*D(I)**3
      DN(I,1)=AM*RO(I)*HI/DMI*DT
      DD(I,1)=D(I)
      IF(AM.LT.1.E-10) DD(I,1)=0.
C
C  COMPUTE THE DROPLET BURNING RATES,HEAT OF COMBUSTION,AND HEAT TRANSFERRED.
C
      DO 19 J=1,JJ
      TSS(J)=0.
      RE(J)=0.
      BRF(J)=0.
      QIN(J)=0.
      QC(J)=0.
   19 QG(J)=0.
      TS(I,1)=TSI+273.
      DO 20 J=1,JJ
      DM(I,J)=A*DD(I,J)**3
      IF(DD(I,J).LT.1.E-10) GO TO 20
      RE(J)=VF(I,J)*DD(I,J)*RHOG/MUG
      A1=SQRT(RE(J))
      DMT=DM(I,J)/DT
      IF(TS(I,J).GE.T9) GO TO 601
      BRF(J)=CDP*YOC*3.14159*DD(I,J)*(2.+0.6*A1*SC**0.3333)*32./AI
      IF(BRF(J).GT.DMT) BRF(J)=DMT
      QC(J)=HC*BRF(J)
      QG(J)=3.14159*AKG*DD(I,J)*(TS(I,J)-TG)*(2.+0.6*A1*A2)
      QIN(J)=QC(J)-QG(J)
      GO TO 602
  601 BR=2.*3.14159*DD(I,J)*AKG/CPG*ALOG(1.+B)
      IF(BR.LT.1.E-10) BR=0.
      BRF(J)=BR*(1.+0.3*A1*A2)
      IF(BRF(J).GT.DMT) BRF(J)=DMT
      QIN(J)=HFG*BRF(J)
      QC(J)=HC*BRF(J)
      QG(J)=QC(J)-QIN(J)
      TS(I,J)=T9
  602 IF(J.EQ.JJ) GO TO 605
      BRS=BRS+BRF(J)*DN(I,J)
      Q=Q+QG(J)*DN(I,J)
  605 TSS(J)=TS(I,J)-273.
   20 CONTINUE
C
      IF(N.LT.NPRT) GO TO 1001
      IF(IQ.NE.1) GO TO 1001
      PRINT 501,I
      PRINT 502,(DD(I,J),J=1,JJ)
      PRINT 503
      PRINT 504,(DN(I,J),J=1,JJ)
      PRINT 503
      PRINT 515,(TSS(J),J=1,JJ)
      PRINT 503
      PRINT 505,(RE(J),J=1,JJ)
      PRINT 503
      PRINT 511,(BRF(J),J=1,JJ)
      PRINT 503
      PRINT 506,(QIN(J),J=1,JJ)
      PRINT 503
```

```
      PRINT 507,(QC(J),J=1,JJ)
      PRINT 503
      PRINT 508,(QG(J),J=1,JJ)
      PRINT 503
 1001 CONTINUE
      KJ=JJ-1
C
C  COMPUTE DROP SIZE,NUMBER,AND TEMPERATURE AT NEXT TIME STEP.
C
      DO 120 K=1,KJ
      KK=JJ+1-K
      IF(DD(I,KK-1).LT.1.E-10) GO TO 110
      IF(TS(I,KK-1).GE.TB) GO TO 604
      CPL=0.34324-1.3869E-4*(TS(I,KK-1)-273.)+1.1044E-7*
     1(TS(I,KK-1)-273.)**2
      B1=QIN(KK-1)/(DM(I,KK-1)*CPL)
      TS(I,KK)=TS(I,KK-1)+B1*DT
      GO TO 603
  604 TS(I,KK)=TS(I,KK-1)
  603 DDM=BRF(KK-1)*DT
      DMD=DM(I,KK-1)-DDM
      IF(DMD.LT.1.E-10) GO TO 110
      DD(I,KK)=(DMD/A)**0.3333
      DN(I,KK)=DN(I,KK-1)
      GO TO 120
  110 DD(I,KK)=0.
      DN(I,KK)=0.
      TS(I,KK)=0.
  120 CONTINUE
   10 CONTINUE
  501 FORMAT(5X,"I=",I3/)
  502 FORMAT(10X,"DD",2X,10E11.4)
  503 FORMAT(/)
  504 FORMAT(10X,"DN",2X,10E11.4)
  505 FORMAT(10X,"RE",2X,10E11.4)
  506 FORMAT(10X,"QIN",2X,10E11.4)
  507 FORMAT(10X,"QC",2X,10E11.4)
  508 FORMAT(10X,"QG",2X,10E11.4)
  511 FORMAT(10X,"BRF",2X,10E11.4)
  515 FORMAT(10X,"TS",2X,10E11.4)
      RETURN
      END
      SUBROUTINE BALANCE
C
C  THIS SUBROUTINE DOES HEAT AND MASS BALANCES.
C
      COMMON /NMRH/DT,MOLO,MOLG,R,TG,VOL,YOC
      COMMON /NRB/AI,BRS,P,Q
      COMMON /MRR/RHOG,GM,VF(11,600)
      COMMON /NR/ALI,CPS,QW,TW
      REAL MOLO,MOLG,MUG,MRO
      F(X,Y)=(2-W*(X-Y))*V
      G(X,Y)=W*(X-Y)*S
C
C  MASS BALANCE ON GAS.
C
      CPG=0.2316+4.61E-5*TG
      CVG=CPG/1.4
      MUG=4.2E-6*TG**0.66
      AKG=1.05E-6*TG**0.71852
      MRO=AI*BRS*DT/32.
      MOLO=MOLO-MRO
      MOLG=MOLG-MRO
```

```
      YOC=MOLO/MOLG
      IF(YOC.LT.1.E-12) YOC=0.
C
C  USE OF HEAT BALANCE EQUATIONS TO EVALUATE GAS AND WALL TEMPERATURES.
C
      HH=0.000054
      W=HH*ALI
      V=1./(RHOG*VOL*CVG)
      S=1./(ALI*CPS)
      QW=W*(TG-TW)
C
C  USE OF RUNGE-KUTTA METHOD TO SOLVE FOR GAS AND WALL TEMPERATURES.
C
      A1=F(TG,TW)*DT
      B1=G(TG,TW)*DT
      A2=F(TG+A1/2.,TW+B1/2.)*DT
      B2=G(TG+A1/2.,TW+B1/2.)*DT
      A3=F(TG+A2/2.,TW+B2/2.)*DT
      B3=G(TG+A2/2.,TW+B2/2.)*DT
      A4=F(TG+A3,TW+B3)*DT
      B4=G(TG+A3,TW+B3)*DT
      TG=TG+(A1+2.*A2+2.*A3+A4)/6.
      TW=TW+(B1+2.*B2+2.*B3+B4)/6.
      P=MOLG*R*TG/VOL
      RETURN
      END
```

REPORT DISTRIBUTION

Mr. Harry Alter, Chief (1)
Safety Analysis Branch
Division of Reactor Development
and Demonstration
Department of Energy
Washington, D. C. 20545

Assistant Director for Reactor (1)
Safety
Division of Reactor Development
and Demonstration
Department of Energy
Washington, D. C. 20545

Dr. Raymond Alcouffe (1)
Los Alamos Scientific Laboratory
Mail Stop 269
P. O. Box 1663
Los Alamos, N. M. 87545

Dr. Robert Avery, Director (2)
Reactor Analysis & Safety
Division
Argonne National Laboratory
9700 South Cass Avenue
Argonne, Illinois 60439

Dr. L. W. Caffey, Director (1)
CRBR Plant Project Office
Department of Energy
P. O. Box U
Oak Ridge, Tennessee 37830

Dr. R. Curtis, Chief (1)
Analytical Advanced Reactor
Safety Research Branch
Nuclear Regulatory Commission
Washington, D. C. 20555

Dr. William Davey (1)
Q Division Leader
Mail Stop 561
Los Alamos Scientific Laboratory
P. O. Box 1663
Los Alamos, N. M. 87545

Dr. Carl A. Erdman (1)
Department of Nuclear Engineering
University of Virginia, Thornton Hall
Charlottesville, Virginia 22901

Dr. R. Ferguson, Director (1)
Fast Flux Test Facility Project Office
Department of Energy
P. O. Box 550
Richland, Washington 99352

Mr. Domenic Vassallo, Acting Director (1)
Division of Project Management
Nuclear Regulatory Commission
Washington, D. C. 20555

Mrs. H. Gearin, Licensing (1)
Assistant for Special Projects
Division of Project Management
Nuclear Regulatory Commission
Washington, D. C. 20555

Mr. C. R. Hahn, Manager (1)
Fuels Design and Development
Pacific Northwest Laboratories
P. O. Box 999
Richland, Washington 99352

Dr. Stephen H. Hanauer (1)
Technical Advisor
Office of the Executive Director
for Operations
Nuclear Regulatory Commission
Washington, D. C. 20555

Mr. K. Hikido, Manager (1)
General Electric Company
Systems Evaluation & Safety
Engineering
Fast Breeder Reactor Department
310 DeGuigne Drive
Sunnyvale, California 94086

Dr. Harry Hummel (1)
Applied Physics Division
Argonne National Laboratory
Building 208
9700 South Cass Avenue
Argonne, Illinois 60439

Dr. Vijen Javeri (1)
Fast Reactor Accident Analysis
Gesellschaft fur Reaktorsicherheit
(GRS) mbH
Glockengasse 2·5000 Koln 1
West Germany

Dr. William Kastenberg (1)
Department of Chemical Nuclear
and Thermal Engineering
University of California
at Los Angeles
Los Angeles, California 90024

Dr. C. N. Kelber, Assistant Director (2)
for Advanced Reactor Safety Research
Division of Reactor Safety Research
Nuclear Regulatory Commission
Washington, D. C. 20555

Mr. Richard Lorenz (1)
Air/Ground Explosions Division
Naval Surface Weapons Center
White Oak
Silver Spring, Maryland 20910

Dr. Roger J. Mattson, Director (1)
Division of Systems Safety
Office of Nuclear Reactor Regulation
Nuclear Regulatory Commission
Washington, D. C. 20555

Dr. James F. Meyer (15)
Advanced Reactors Branch
Division of Project Management
Nuclear Regulatory Commission
Washington, D. C. 20555

Professor F. J. Munno (1)
Nuclear Engineering Program
Department of Chemical
Engineering
University of Maryland
College Park, Maryland 20745

Dr. David Okrent (1)
Department of Chemical Nuclear and
Thermal Engineering
University of California
at Los Angeles
Los Angeles, California 90024

Mr. Frank E. Panisko, Senior (1)
Development Engineer
Fuels Design and Development
Pacific Northwest Laboratories
P. O. Box 999
Richland, Washington 99352

Mr. D. F. Ross, Assistant Director (1)
for Reactor Safety
Nuclear Regulatory Commission
Washington, D. C. 20555

Secretary, Advisory Committee on (5)
Reactor Safeguards
Nuclear Regulatory Commission
Washington, D. C. 20555

Dr. Arkal S. Shenoy, Manager (1)
Systems & Safety Analysis
Branch
Gas Cooled Fast Breeder Reactor
General Atomic Company
P. O. Box 81608
San Diego, California 92138

Mr. M. Silberberg, Chief (1)
Experimental Fast Reactor
Safety Research Branch
Division of Reactor Safety Research
Nuclear Regulatory Commission
Washington, D. C. 20555

Mr. Daniel E. Simpson (1)
Manager, Safety Engineering
Hanford Engineering Development
Laboratory
P. O. Box 1970
Richland, Washington 99352

Dr. Themis P. Speis, Chief (1)
Advanced Reactors Branch
Division of Project Management
Nuclear Regulatory Commission
Washington, D. C. 20555

Dr. Michael Stevenson (2)
Los Alamos Scientific Laboratory
P. O. Box 1663
Los Alamos, N. M. 87545

Dr. David Swanson (1)
Materials Sciences Laboratory
Aerospace Corporation
P. O. Box 92957
Los Angeles, California 90009

Technical Information Center (1)
Nuclear Regulatory Commission
P. O. Box 62
Oak Ridge, Tennessee 37830

Dr. Theo G. Theofanous (1)
132 Pathway Lane
Lafayette, Indiana 47906

Dr. J. V. Walker, Dept. Manager (1)
Reactor Research and Development
Sandia Laboratories
P. O. Box 5800
Albuquerque, N. M. 87115

	BNL Distribution
DNE Chairman	(1)
DNE Deputy Chairman	(1)
RSP Associate Chairmen	(3)
SEG/EARS Division	(6)
Nuclear Safety Library	(2)